journal of the international meteor organization

WGN

46:6
december 2018

Eta Virginids four year cycle
BRAMON search method for meteor radiants
Velocity calculation of a meteoroid that generates a head echo
Visualizing sporadic radio meteor radiants and their dynamics
January IMO video meteors
Meteor reports in The Astronomer magazine - part III

ISSN 1016-3115

WGN Vol. 46, No. 6, December 2018, pp. 183 – 216

Administrative

Meteor Science

Radio meteors

Preliminary results

History

Front cover photo

Fireball over Topaz Lake, CA, photographed on 2014 December 13, using Canon EOS 5D Mark III, 16 mm $f/2.8$ lens, and 25 s exposure at ISO 6400. Image courtesy: Jeff Sullivan.

Writing for WGN

This Journal welcomes papers submitted for publication. All papers are reviewed for scientific content, and edited for English and style. Instructions for authors can be found in WGN **45:1**, 1–5, and at `http://www.imo.net/docs/writingforwgn.pdf` .

Copyright

Legal address

International Meteor Organization, Jozef Mattheessensstraat 60, 2540 Hove, Belgium.

From the Treasurer — IMO Membership/WGN Subscription Renewal for 2019

Marc Gyssens

Renewal rates

Most members/subscribers whose membership/subscription has expired should have received a reminder email or should receive one shortly. Via this way, we invite them again to renew for 2019.

The fees are as tabulated below. We are happy that we can offer WGN at the same cost in Euros as last year and that we can lower some of the US Dollar equivalents. We also continue to offer an electronic-only subscription at a reduced rate.

IMO Membership/WGN Subscription 2019				
Electronic + paper with surface mail delivery:		€26		US$ 32
Electronic + paper with airmail delivery (outside Europe only):		€49		US$ 60
Electronic only:		€21		US$ 25
Supporting membership:	add	€26	add	US$ 32

It is also possible to renew for two or more years in a row.

When you renew, give a few minutes of thought to becoming a **supporting member** by paying at least 26 EUR/32 USD extra. Smaller gifts are of course also appreciated. As you may know, there is an IMO Support Fund. With this Support Fund, we offer support to meteor-related projects. Our ability to provide this service to the meteor community depends primarily on the gifts we receive from supporting members!

Another way to help meteor workers with limited funds is to offer them a gift subscription.

We already thank all our members that will renew for their continued trust in our Organization!

Other membership benefits

The IMO Council is seeking to expand the benefits of memberships.

Last year, it was decided that the IMO's *Handbook for Meteor Observers* and *Meteor Shower Workbook* are available for free to IMO members in digital form. In this way, IMO members have at their disposal these two invaluable tools to prepare an observing session and to interpret its results. To access these publications, go to the IMO website and click on the menu item "Free Meteor Books" under the tab "Resources".

Also, International Meteor Conference (IMC) participants becoming an IMO member or renewing their IMO membership at the IMC get a reduction of 5 EUR for the next year of membership. While this measure has been taken primarily to encourage IMC participants who are not yet an IMO member to become one, established IMO members also get a small advantage each time they attend an IMC.

We intend to expand membership benefits even further in the near future.

Payment instructions

If you are not yet familiar with the new IMO website, you first must log in into your account if you want to renew. For this purpose, click the log-in button in the upper right-hand corner. As login, use the email address on which you received or will receive my reminder email. In case you forgot your password, you can use the "forgot password" link to reset it. Once logged in, you will see your profile picture (or the space provided for it). If you read on the green button below it that your membership has expired, click it, and the rest will be self-explanatory.[1]

The outcome of this process is that you will see the total amount due and your payment options. If you choose to pay using PayPal (or using a credit card via PayPal), you can complete the payment on our website.

If you experience any difficulties, do not hesitate to contact me at `treasurer@imo.net`.

One final request: every year, a lot of members renew late. As a consequence, back issues that already appeared have to be sent out to these members. Please support our volunteers in their bimonthly effort to have WGN shipped to you by renewing promptly! Thank you for your understanding and cooperation!

[1] Alternatively, you can also click on "Extend your membership" in the pull-down menu to the right of your name in the upper right-hand corner, with the same result.

Meteor Science

Eta Virginids (EVI) four year cycle

Yasuo Shiba [1]

The eta Virginids (EVI; #11) were researched by using Japanese automatic TV meteor observation network (SonotaCo network) data between 2007 and 2018. The results showed that EVI activity increased at intervals of four years. IAU photographic meteor orbit database (IAU MDC) data also indicate a four year cycle after 1942. The four year cycle can be estimated to correspond to encounters with a concentrated meteoroid "swarm" which is generated by the 3:1 resonance with Jupiter. EVI fireballs show a trend of having lower luminous end heights.

Received 2018 October 31

1 Introduction

The eta Virginid meteor shower (IAU #11 EVI) produces a few meteors in mid March in the solar longitude interval from 350° to 5° with a maximum around 357° (Jenniskens et al., 2016). The visually observed Zenithal Hourly Rate (ZHR) is 2 or 3 (Kronk, 1988). EVI is a part of a meteor shower, the so called "Virginid Complex" (Kronk, 1988) between February and April for which historical observations are described in the 19th century (Denning, 1899). Eta Virginid meteor orbits had been recorded by early photographic observations in the "Harvard Meteoric Program" around the 1940s (Letfus, 1955).

2 Observation Data

This research depends on data from the Japanese automatic meteor observation network, the "SonotaCo network". I downloaded SonotaCo data from the daily upload site[a] where analyzed meteor data is put by each observer. The used data period is from 2007 to 2018. The solar longitude interval is from 350 to 5° for radiant distribution research; and from 340 to 10° (J2000.0) for meteor number aggregates and orbital element distributions (see Figures 4–7 later).

Additionally, eta Virginid meteors were selected from the IAU meteor database of photographic orbit data (Neslusan, 2016) by using the D_d criterion (Drummond, 1981). To apply the D_d criterion, orbits were referred to an eta Virginid standard orbit determined by SonotaCo network observations.

3 Results

Distributions of radiant positions, corrected for zenith attraction, on SonotaCo network data are shown in Figure 1 where data are plotted covering intervals from 350° to 5° in solar longitude, from −15° to +15° in declination and from 165° to 200° in right ascension; these plots include meteors over all ranges of velocity. As a result, a significant EVI radiant concentration is shown clearly with a four year period. The most active years are 2009, 2013 and 2017 (labeled "phase 3" below). One year later, in 2010, 2014 and 2018, weak concentrated radiants are also visible (labeled "phase 4" below). No concentrated radiants are found in other years, labeled "phase 1" and "phase 2".

Mean orbital elements are shown in Table 1 that are calculated from the radiant concentrations (selecting meteors by applying the D_d criterion) in 2009, 2013 and 2017. Column headings from the left are as follows: "R.A." is corrected radiant position right ascension [deg], "Decl" is corrected radiant declination [deg], V_g is geocentric velocity [km/s], a is orbital semi-major axis [AU], q is perihelion distance [AU], e is eccentricity, p is orbital period [yr], "peri" is perihelion argument [deg], "node" is accending node [deg] and "incl" is inclination [deg].

Corrected radiant position drift is below, where $\lambda_\odot$ is solar longitude (J2000.0):

$$\begin{aligned} \text{R.A.} &= 0.798(\lambda_\odot - 356.45) + 184.24 \\ \text{Decl} &= -0.152(\lambda_\odot - 356.45) + 2.86 \\ V_g &= -0.09(\lambda_\odot - 356.45) + 26.28 \end{aligned}$$

Next, for "phase 4" and "phase 1+2", EVI meteors were selected by using the D_d criterion (Drummond, 1981) based on Table 1 orbital elements and using the limiting value $D_d < 0.105$. Mean orbital elements for selected meteors are shown in Table 2. Radiant drifts are, for phase 4:

$$\begin{aligned} \text{R.A.} &= 0.800(\lambda_\odot - 357.86) + 187.54 \\ \text{Decl} &= -0.339(\lambda_\odot - 357.86) + 0.85 \\ V_g &= -0.01(\lambda_\odot - 357.86) + 26.53 \end{aligned}$$

and for phase 1+2:

$$\begin{aligned} \text{R.A.} &= 0.882\ (\lambda_\odot - 356.96) + 186.84 \\ \text{Decl} &= -0.0497(\lambda_\odot - 356.96) + 0.57 \\ V_g &= -0.05(\lambda_\odot - 356.96) + 26.44 \end{aligned}$$

Note that when EVI meteor activity is weaker, orbital inclinations are relatively lower.

Numbers of meteors selected as EVI, and mean luminous magnitude, are shown in Table 3 using data that lasted from 350° to 5° in $\lambda_\odot$. Table 3 headings are from left, year of observation, sporadic meteor number, EVI meteor number, ratio of EVI meteors to sporadic meteors (percent), EVI meteors mean absolute

[1]SonotaCo Network, Japan.

IMO bibcode WGN-466-shiba-evi
NASA-ADS bibcode 2018JIMO...46..184S

[a]http://sonotaco.jp/forum/viewforum.php?f=15

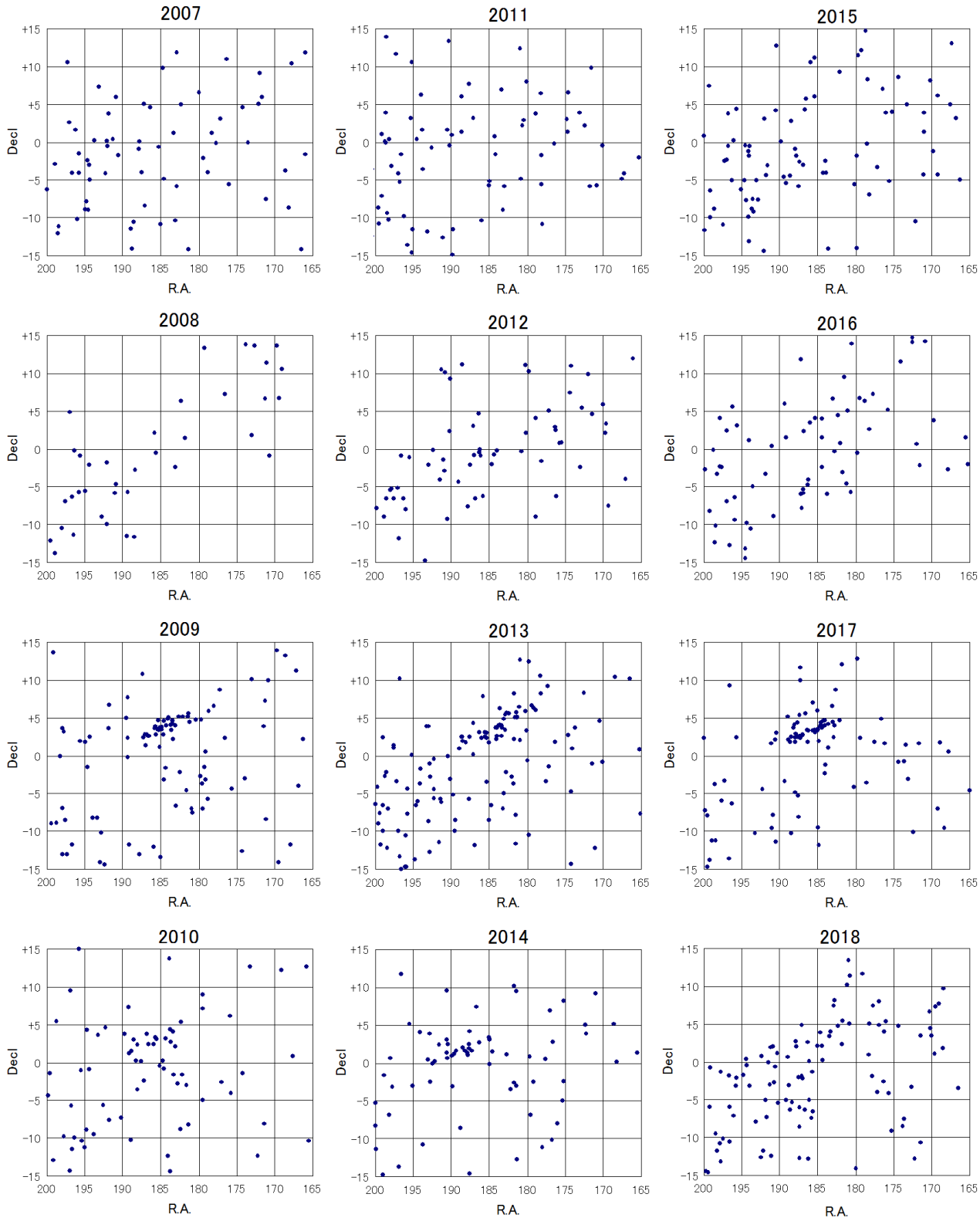

Figure 1 – Radiant distribution in individual years.

Table 1 – EVI mean orbital elements (years corresponding to Phase 3).

R.A.	Decl.	V_g	a	q	e	p	peri	node	incl
184.243	2.863	26.589	2.341	0.455	0.8057	3.58	282.56	356.45	5.19

Table 2 – EVI mean orbital elements (Phase 4 and Phase 1+2).

	R.A.	Decl.	V_g	a	q	e	p	peri	node	incl
Phase 4	185.829	1.571	26.547	2.241	0.449	0.800	3.35	283.70	357.86	4.89
Phase 1,2	181.161	2.078	26.590	2.400	0.459	0.809	3.71	281.88	356.96	4.35

Table 3 – Meteor numbers and mean absolute magnitude.

Year	Sporadic	EVI	EVI/Sp[%]	Mag(EVI)	Mag(Sp)
2007	354	8	2.26	+0.07	−0.34
2008	192	4	2.08	−0.44	−0.47
2009	496	60	12.10	−0.66	−0.41
2010	338	14	4.14	−0.14	−0.53
2011	349	2	0.57	−0.52	−0.52
2012	352	9	2.56	−0.52	−0.71
2013	561	33	5.88	−0.39	−0.38
2014	347	19	5.48	−0.69	−0.77
2015	467	5	1.07	−0.25	−0.61
2016	360	5	1.39	−0.00	−0.71
2017	374	36	9.63	−1.00	−0.50
2018	545	35	6.42	−0.95	−0.49

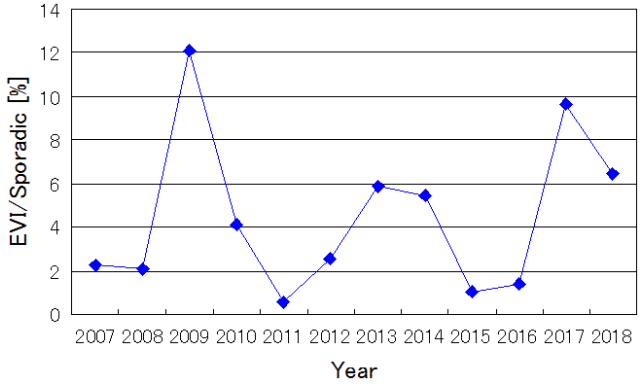

Figure 2 – Ratios of EVI to sporadic.

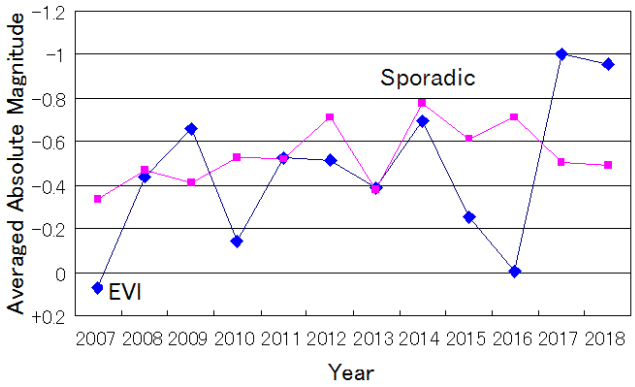

Figure 3 – Mean absolute magnitude of EVI and sporadic.

magnitude and sporadic meteors mean absolute magnitude. Sporadic meteors were selected from the same solar longitude range as EVI (with no limits in radiant and V_g). The ratios of EVI meteors to sporadic meteors are shown in Figure 2. EVI and sporadic meteors mean absolute magnitude are shown in Figure 3.

EVI meteor ratios increased in 2009 and 2017 especially (Figure 2), while in 2018, 2013 and 2014 EVI were somewhat numerous. This result indicates that EVI activity increases at intervals of every four years. The years 2009, 2017 and 2018, when EVI numbers increased, show bright EVI mean absolute magnitudes.

The ratio of EVI meteor numbers to sporadic meteors for 1° bins in $\lambda_\odot$ are shown in Figures 4, 5 and 6 respectively for phase 1+2, phase 3 and phase 4.

No peaks are found at phase 1+2 (2007, 2008, 2011, 2012, 2015, 2016: Figure 4). Phase 1 and 2 data indicate that in fact we observed a part of the "Anti-helion" meteors that radiate from around the zodiacal area in late February to April that were however classified as EVI. Phase 3 (2009, 2013, 2017: Figure 5) shows a clear

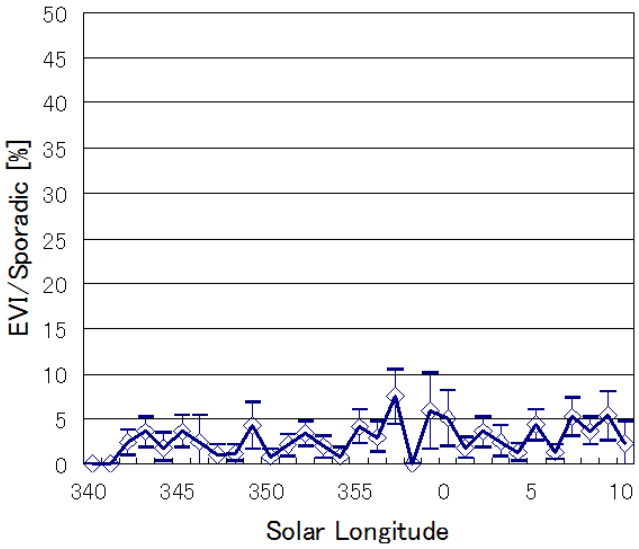

Figure 4 – Activity profile of Phase 1+2.

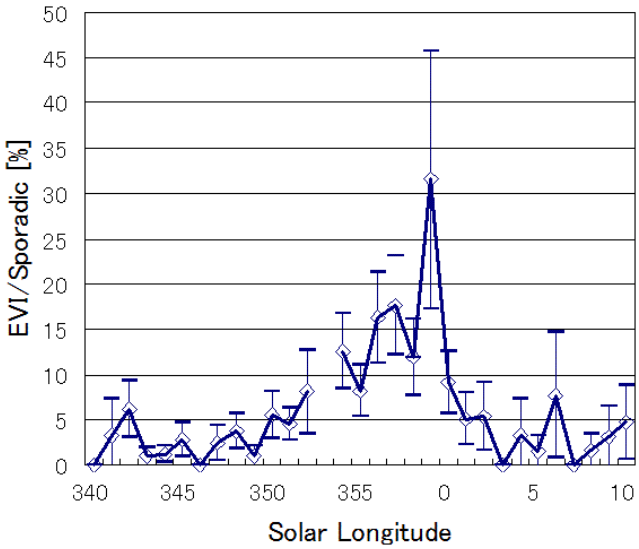

Figure 5 – Activity profile of Phase 3.

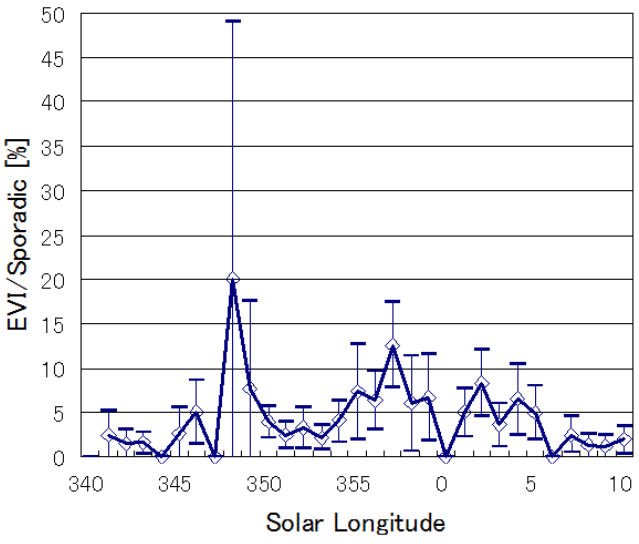

Figure 6 – Activity profile of Phase 4.

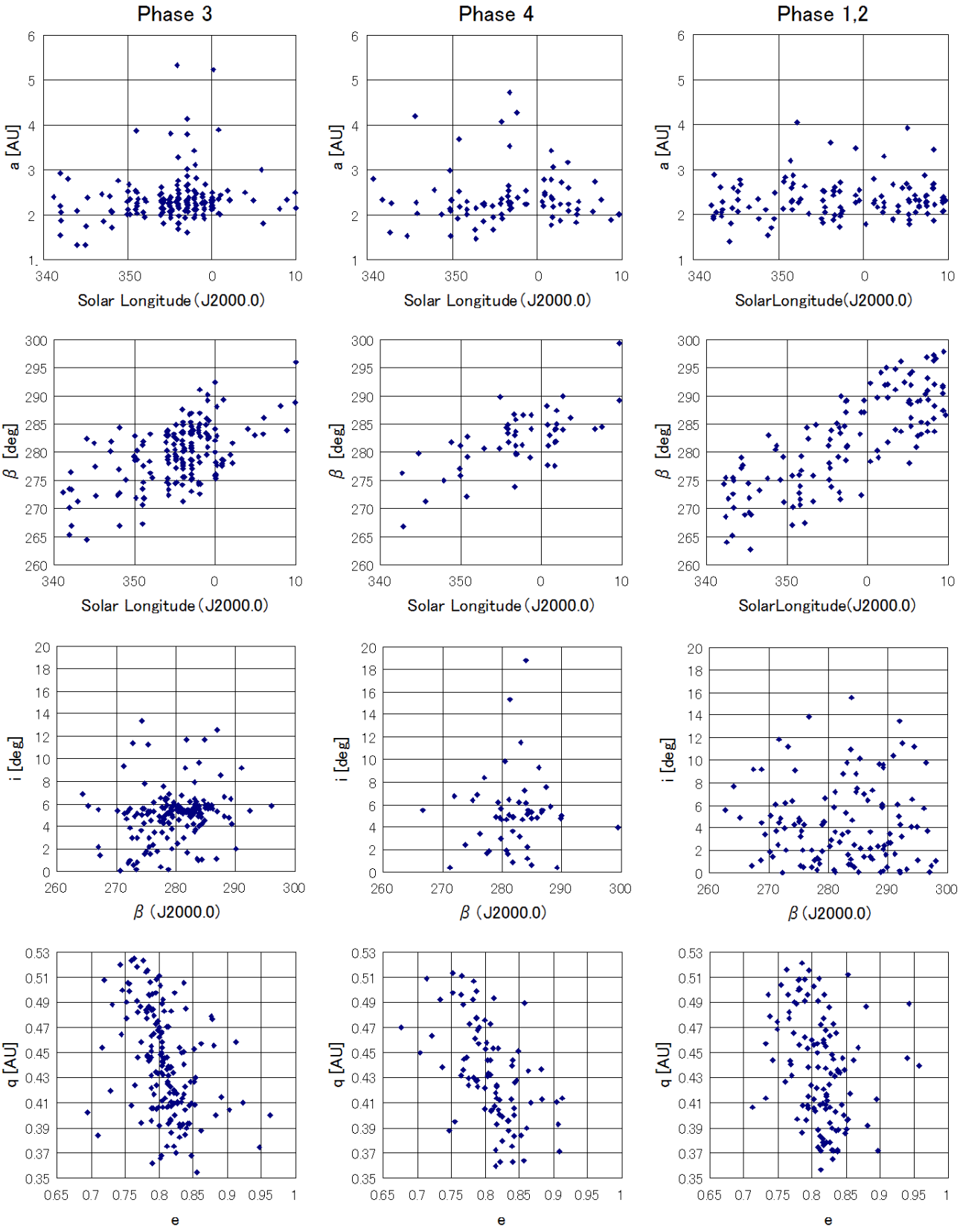

Figure 7 – Some orbital element distributions of EVI.

EVI peak from 350° to 6°. Maximum is at 357–359° and meteor numbers are about five times as high as phase 1+2. Phase 4 EVI active duration is from 354° to 6° and maximum is around 357° (Figure 6). Maximum meteor rate is two times that of phase 1+2. In Figure 6, the meteor rate at $\lambda_{\odot}$=348° increased but note the very large error bar.

Figure 7 shows some orbital elements, from left to right, phase 3, phase 4 and phase 1+2. From the top, semi-major axis versus solar longitude, ecliptic longitude of the orbit's perihelion vs solar longitude, inclination vs ecliptic longitude of perihelion and perihelion distance vs eccentricity. The phase 3 distributions have clear concentrations, however the distributions in ev-

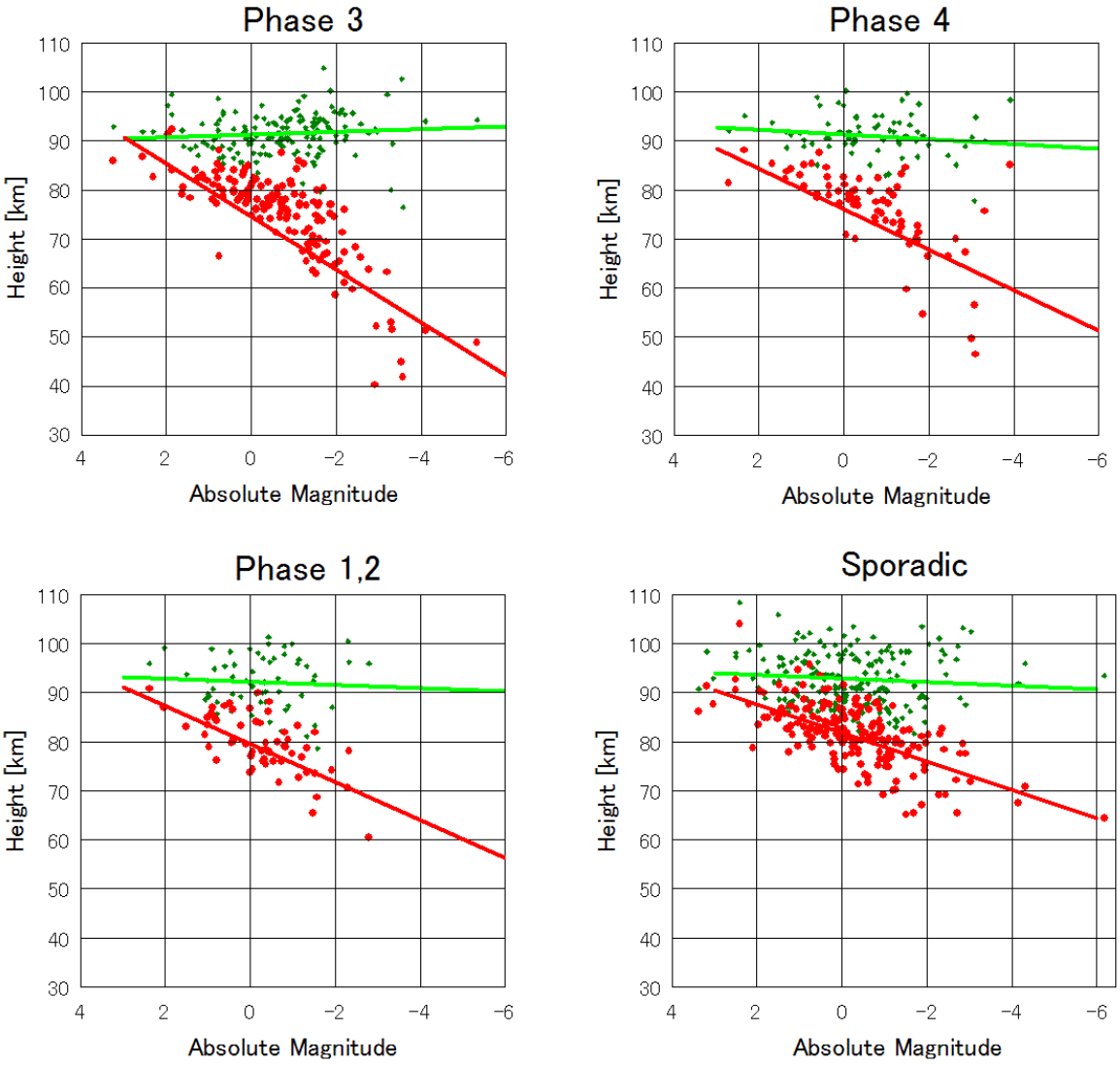

Figure 8 – Beginning and ending heights.

ery phase 1+2 plot are sparse. Phase 4 indicates weak phase 3 characteristics added to phase 1+2 features.

Figure 8 is the distribution of beginning (small green dots) and end heights (large red dots) against absolute magnitude for EVI and sporadic meteors. Sporadic meteors are selected here in a similar geocentric velocity range to EVI, that is from 25 till 29 km/s and mean velocity is 26.8 km/s. Beginning and end height individual linear approximations are added in Figure 8. Characteristic EVI bright meteors show especially low ending heights that are considered high mechanical strength meteoroids.

The radiant distributions of meteors decided to be EVI are shown in Figure 9 for phase 3, phase 4 and phase 1+2 individually. Figure 9 indicates that the concentrated radiants on the northern side of the zodiacal line at phase 3 are not found in phase 1,2. Additionally, the diffuse radiant distribution on the south side of the zodiacal line, visible in phase 3, is also difficult to find in phase 1+2. It is possible that a Jovian resonance southern branch accompanies the EVI.

EVI meteors were selected using the D_d criterion ($D_d < 0.105$) from the IAU MDC (Meteor Data Center) photographic orbit database (Neslusan, 2016) and the result is shown in Figure 10 for individual years. A four year interval is labeled on the Figure 10 horizontal axis. Many meteors are recorded at this four year interval.

4 Discussion

Total EVI meteors are 230 in the SonotaCo network's twelve years of observations (Table 3). EVI is a minor meteor shower and detailed statistical analysis was difficult because recorded meteor numbers are not so many. I hope additional meteor data will be obtained by future observations so that we can progress detailed analysis.

The SonotaCo network's twelve years of observations (Figures 1, 2, 4, 5 and 6) and photographic observations since the 1940s (Figure 10) indicate that the eta Virginid meteor shower (EVI) has enhanced activity at four year intervals. However the EVI orbital period does not agree well enough with the shorter period derived from observational results, namely 3.58 yr (Table 1). This difference will be due to orbit calculation error. The relations of semi-major axis and orbital period with the end point altitude on phase 3 EVI meteors are shown in Figure 11. The orange line with increas-

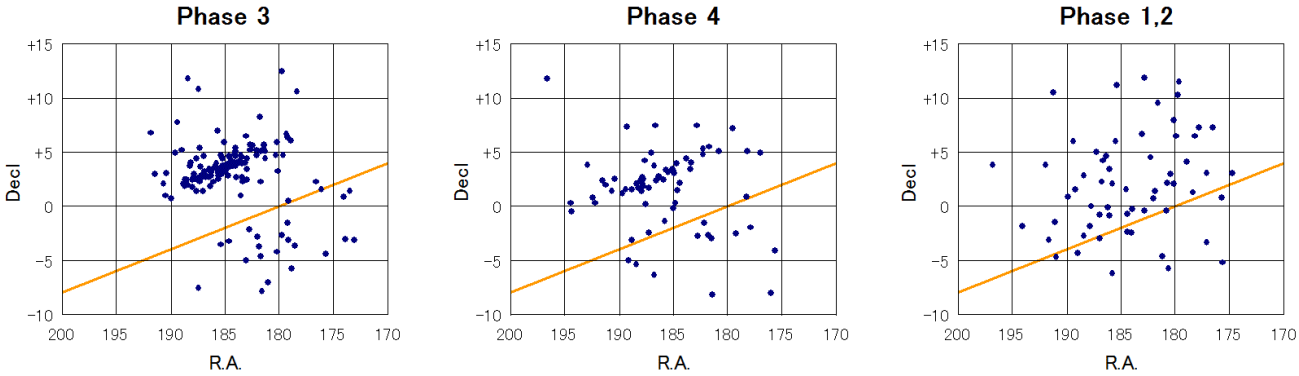

Figure 9 – Radiant distributions of EVI for each phase. The line is the ecliptic.

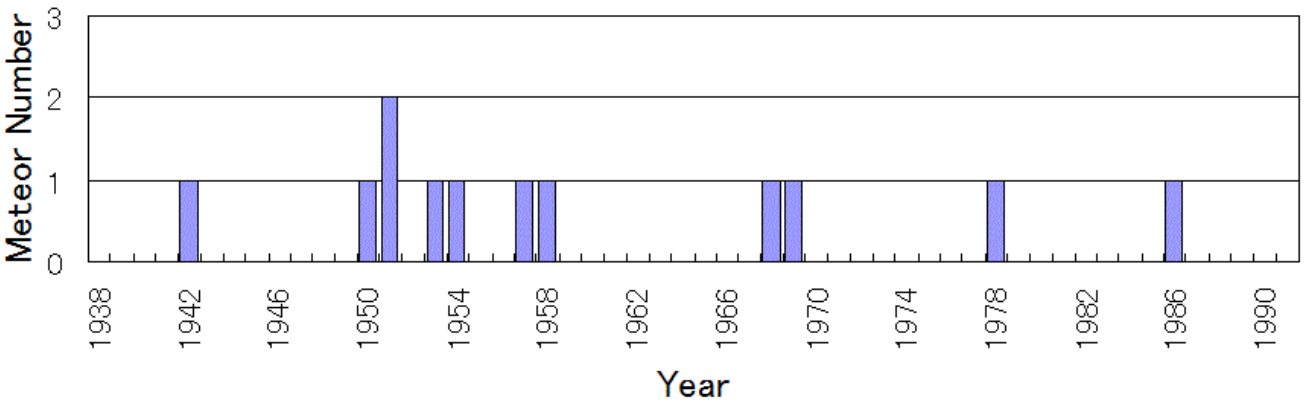

Figure 10 – EVI meteor numbers recorded in the IAU MDC photographic orbit database.

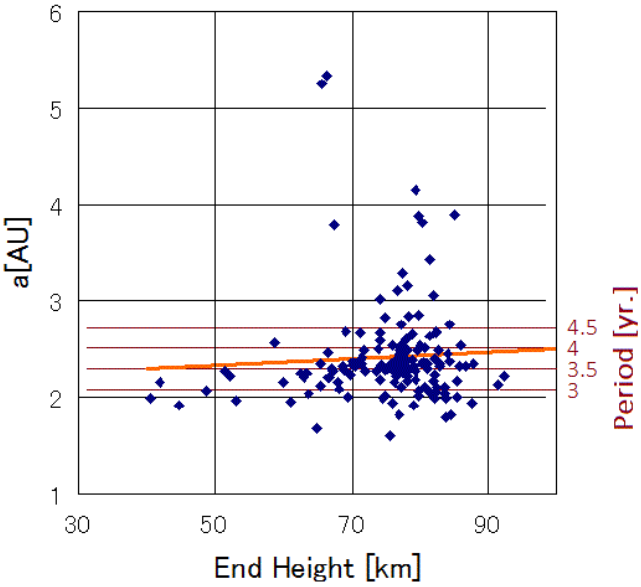

Figure 11 – Semi-major axis against end height.

ing slope in Figure 11 is a linear approximation which indicates a positive correlation. If slow velocity meteoroids collide with the Earth and reach low altitude, a clear deceleration on the terminal part of the trajectory is generally observed. Orbital calculation software UFOOrbit calculates meteor velocity from mean angular velocity. Therefore slow velocity and low ending height meteors, like EVI, show a trend of slower velocity estimation (Figure 11). That effect leads to results of shorter orbital period than the true period. If this error has an influence, EVI can be considered to fall into the 3:1 resonance (3.954 yr) with Jupiter's orbit. As a result, a meteoroid concentration named a "swarm" (Asher & Izumi, 1998) is formed and can explain the four year periodic activity. The resonance period is slightly shorter than four years, and as a result, four years later we will observe the swarm phase as being 17° earlier. This difference will produce an 87 year grand period (22 resonant cycles). If we estimate that we encountered the swarm center at 2009.35 (since the swarm center existed between 2009 and 2010 from the observational results, and nearer to 2009), the Earth previously encountered the swarm center at 1954 (14 cycles of the resonant swarm period earlier). Photographic observation results (Figure 10) look like a little enhancement may be recorded at that time but it is uncertain because the observation quantity is small. The second previous older grand maximum at 1867 occurred at an early stage of meteor science. Denning (1899) described "many fireballs" for Virginids. However it is unknown which of the eta Virginids or any other Virginids are referred to by his "Virginids". And additionally, the observed year of "many fireballs" was not described. I could not find the 87 year grand period from previous observation reports. We will encounter the swarm center in future at 2037 or 2041. At those chances, we expect to observe many spectacular EVI fireballs with long trails.

On the other hand, almost no EVI were observed in 2007, 2008, 2011, 2012, 2015 and 2016. In these years the meteors selected as EVI meteors by the D_d criterion

(Figure 9: phase 1,2) can be presumed to be part of the "anti-helion" (Rendtel, 2017) meteors that have similarities with EVI orbits. In conclusion, phase 1 and phase 2 EVI meteors are not exactly EVI meteors but a part of the anti-helion meteor source (Rendtel, 2017), because in Figures 1, 4, 7 and 9, any concentration whose existence would suggest a meteor shower cannot be found. In the Virginid complex (McBeath, 1992), the most important structure is explained in terms of the synthesis of two components. One is anti-helion meteors as an annual meteor shower from February to April, the other is true EVI meteors showing a four year cycle enhancement. This differs from the explanation of Molau et al. (2013) that described a synthesis of three meteor showers from February to April.

Phase 3 and phase 4 EVI meteor orbits are almost the same (Figure 7). The whole observed part of a swarm (Asher & Izumi, 1998) orbit features differences but these are within observational error.

The magnitude of EVI meteors in clearly active years is brighter than other years (Figure 3). Typical end heights of bright EVI meteors are lower than sporadic meteors (Figure 8). EVI swarm (phase 3 and 4) meteoroids were larger and of higher mechanical strength than sporadic meteoroids. Anti-helion meteoroids (phase 1 and 2) had intermediate features between EVI and sporadic.

Acknowledgements

This research depended on the SonotaCo network open data source. I thank network operator Mr. SonotaCo and many observers who endeavor to obtain high quality observational data. Mr. M. Koseki advised me about useful literature.

References

Asher D. J. and Izumi K. (1998). "Meteor observations in Japan: new implications for a Taurid meteoroid swarm". *Mon. Not. Roy. Astron. Soc.*, **297**, 23–27.

Denning W. F. (1899). "General catalogue of the radiant points of meteoric showers and of fireballs and shooting stars observed at more than one station". *Mem. Roy. Astron. Soc.*, **53**, 203–292.

Drummond J. D. (1981). "A test of comet and meteor shower associations". *Icarus*, **45**, 545–553.

Jenniskens P., Nénon Q., Albers J., Gural P. S., Haberman B., Holman D., Morales R., Grigsby B. J., Samuels D., and Johannink C. (2016). "The established meteor showers as observed by CAMS". *Icarus*, **266**, 331–354.

Kronk G. W. (1988). *Meteor Showers: A Descriptive Catalog.* Enslow, NJ.

Letfus V. (1955). "The Orbits of the Virginids and κ Cygnids". *Bulletin Astron. Institutes Czechoslovakia*, **6**, 143–146.

McBeath A. (1992). "UK visual results for the Virginids, 1988–1992". *WGN (JIMO)*, **20:6**, 226–237.

Molau S., Kac J., Berko E., Crivello S., Stomeo E., Igaz A., Barentsen G., and Goncalves R. (2013). "Results of the IMO Video Meteor Network – March 2013". *WGN (JIMO)*, **41:3**, 96–100.

Neslusan L. (2016). "IAU Meteor Data Center Photographic and Video Databases Version 2016". `https://www.astro.sk/~ne/IAUMDC/PhV2016/photo.html` .

Rendtel J. (2017). "2018 Meteor Shower Calendar". `http://www.imo.net/files/meteor-shower/cal2018.pdf` . IMO.

Handling Editor: David Asher

A Search Method for Meteor Radiants

Leonardo S. Amaral[1,2], *Carlos A. P. B. Bella*[1,3], *Lauriston S. Trindade*[1,4], *Marcelo L. P. V. Zurita*[1,5], *Gabriel G. Silva*[1,6], *Marcelo W. S. Domingues*[1,7], *Renato C. Poltronieri*[1,8], *Cristóvão J. L. Faria*[1,9], *and Carlos F. Jung*[1,10]

This article presents the results of a study whose goal it was to develop a method to search for new showers. The method inputs are meteor orbits provided by data from video-monitoring networks. As a result, the method proved to be effective in providing a list of new potential showers. The method consists of five data-analysis and processing steps. This study and development provided an important tool for the search of new showers. Up to the present moment, the method enabled the identification of more than a hundred new potential showers.

Received 2018 September 20

1 Introduction

In 2017 the BRAMON (Amaral et al., 2017) meteor video-monitoring network began its search for new meteor showers. This activity led to the research and development of a new method. The search used input orbits of meteors provided by the BRAMON database and by other meteor video-monitoring networks, such as: EDMOND (Kornoš et al., 2014a; Kornoš et al., 2014b; EDMOND, 2018), and SonotaCo (SonotaCo, 2009; SonotaCo, 2018).

2 Description of the Method

The method consists of a processing procedure, split into five steps, which at the end generates a list of new potential showers. The steps comprise of following: 1 – Orbits of sporadic meteors (meteors not belonging to any specific shower (Ceplecha et al., 1998)) are clustered using clustering algorithms like the DBSCAN algorithm (Ester et al., 1996) – *Density-based spatial clustering of applications with noise* (Sugar et al., 2017); 2 – The orbit clusters discovered in the first step undergo a process of combinatorial analysis that groups the orbits that have the characteristics of a shower; 3 – The results of step 2 are then validated against the list of known showers of the IAU Meteor Data Center (MDC, 2018). The resulting product is a collection of orbits that are strong candidates for new showers; 4 – The step 4 candidates undergo a refinement process that looks for additional members of the showers and tries to determine the shower center (average orbit located at the point with the highest concentration of shower orbits), which are then validated against the MDC database; and 5 – New methods are used to better understand the shower and its relation with other nearby showers. The steps of the proposed method are described below:

Step 1 — Finding similar groupings of orbits

A clustering algorithm is used to evaluate a list of previously extracted meteor orbits. In this work the DBSCAN algorithm was used but it could also be used others clustering algorithms (taking advantage of the characteristics of each). To optimize the process only orbits that are classified in the database as sporadic meteors should be used. Each element of the list has the following orbital parameters: RA, DEC, solar longitude, geocentric velocity, semi major axis (a), eccentricity (e), periapsis distance (q), argument of periapsis (ω), longitude of the ascending node (Ω), and inclination (i).

As described in Southworth & Hawkins (1963) the orbit of a meteor can be represented as a point in a 5-dimensional space, and the similarity between them can be assessed by calculating the distance between these points. Thus, the DBSCAN algorithm can be used to separate orbit clusters, and the distance between different orbits is calculated by the similarity between them.

The output of DBSCAN is a set of orbit clusters. The orbits of each cluster are considered to be neighbors and they have similar orbital characteristics.

In order to analyze if one orbit is similar to another, mathematical methods that calculate the orbital dissimilarity between two orbits can be used. These methods measure the extent to which two orbits are dissimilar, i.e., the lower the result, the more the orbits are similar. As an example, the method of Drummond (D), (Drummond, 1981; Galligan, 2001; Jopek et al., 2002) was used, whose implementation of the formula uses the orbital parameters e, q, ω, Ω, and i.

This implementation of DBSCAN uses the D_{maxc}, minPoints, and minClusterSize input parameters, which are described below.

D_{maxc} represents the maximum limit of the D criterion to determine if an orbit is considered a neighbor of another orbit. That is, if the D test returns a value lower than D_{maxc} the two orbits are considered neighbors.

DBSCAN uses the *core point* concept. The minPoints parameter represents the minimum amount of neighbors that a point must have to be considered a *core point*.

[1]BRAMON - Brazilian Meteor Observation Network, Nhandeara, Brazil.
[2]OCA – Observatório Campo dos Amarais, Bilac, Brazil. Email: lsamaral_ios@hotmail.com
[3]Email: carlos.pbella@gmail.com
[4]Email: lauristontrindade@yahoo.com.br
[5]Email: marcelozurita@gmail.com
[6]Instituto de Química, Universidade de São Paulo, São Paulo, Brazil. Email: gabrielg@iq.usp.br
[7]Email: marcelo@casb.com.br
[8]Email: rcpoltronieri@gmail.com
[9]SONEAR – Southern Observatory for Near Earth Asteroids, Oliveira, Brazil. Email: cjacqueslf@gmail.com
[10]HELLER & JUNG – Space and Sky Observatory, Taquara, Brazil. Email: carlosfernandojung@gmail.com

IMO bibcode WGN-466-amaral-radiants
NASA-ADS bibcode 2018JIMO...46..191A

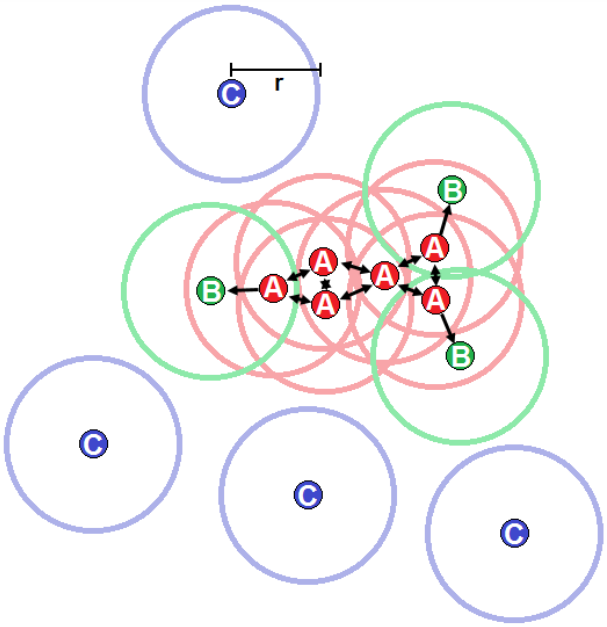

Figure 1 – Red points are *core points* (MinPoints= 3), green points are reachable points, and the blue point is noise. D_{maxc} is represented by the radius of the larger circles.

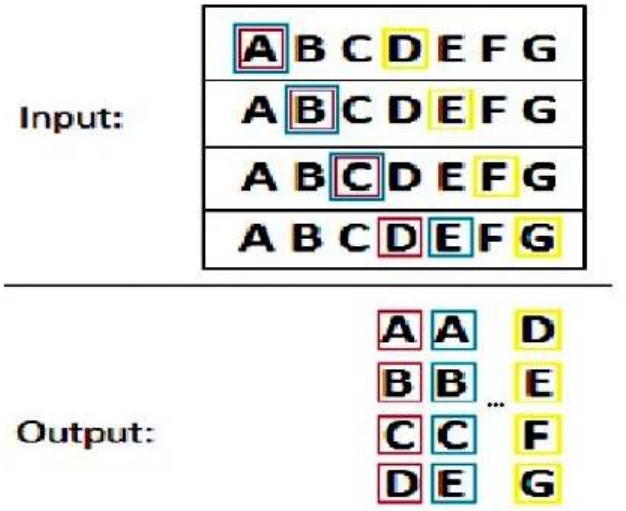

Figure 2 – Representation of the execution of the simple combination algorithm. In this example the orbits are represented by letters (AB. . . G). The input represents a cluster and the output the possible combinations. The ShowerMin parameter is 4.

The minPoints parameter directly impacts how "dense" a set of orbits should be in order to be considered a cluster. Points that are neighbors of a core point, but do not satisfy the minPoints parameter, are also part of the cluster and are called reachable points. Points that are not core points or reachable points are considered noise, see Figure 1.

In order to be considered a cluster, the group comprising the core points and the reachable points must be greater than or equal to the minClusterSize parameter.

Each cluster that is found is not necessarily a shower. It may have no shower or it may have several. This depends on how the orbits are distributed and the parameters used in DBSCAN. The use of a high D_{maxc} can lead to false clusters (obits that are not really similar will be grouped as a cluster). Tests performed indicate that good D_{maxc} values are between 0.04 and 0.07 (Using these values it was possible to find most known showers). Values close to 0.01 and 0.02 can be used to find filaments within dense clusters (This value can dissolve a large clusters in severals small clusters. Only the denser orbits groups survive. In these cases filaments pertaining to the same shower can be exposed).

Step 2 — Combining the Elements of a Cluster

After the clusters are found by DBSCAN, an algorithm that performs a simple combination in each cluster find in Step 1 must be executed. The input parameters of this combination are: Cluster, ShowerMin, ClusterSizeMax, and D_{maxa}.

The ShowerMin parameter defines the size of the groupings that are used by the simple combination algorithm. A cluster smaller than the ShowerMin parameter is discarded. In the tests performed, ShowerMin was configured with values 6 and 8.

The Figure 2 represents the output of a simple combination of an input cluster. In Figure 2 the red, blue, and yellow columns in output represent the results of the first, second, and last iteration of the algorithm, respectively.

Clusters larger than the ClusterSizeMax parameter are split into smaller groups, because the combinatorial analysis algorithm has $N!$ computational complexity, and therefore, very large clusters take a long time to process (we use values under 60 in our tests). However, this number can be increased depending on the available computational power.

Another way to reduce cluster sizes is running DBSCAN with small values of D_{maxc} and larger values of minPoints, as this can break down a large cluster into several smaller ones.

Each grouping found by the combinatorial analysis must undergo a validation test that aims to determine whether they constitute a possible shower or not. In this test, an *average orbit* is generated using all the orbits of the grouping. That is, each parameter (e, q, ω, Ω, and i) of this average orbit is calculated as the mean of the respective parameter of all the orbits of the grouping. A D test is then performed for each of the orbits of the grouping against its average orbit. If the result of each of the D tests of this procedure is lower than the D_{maxa} parameter, this grouping is considered a shower.

Due to the characteristics of this simple combinatorial analysis, the output list of new potential showers may contain several combinations of groupings, which sometimes differ by only a single orbit (like 'ABCD' and 'ABCE' in Figure 2), since they actually belong to a single shower. In this case the groupings can be combined, thus forming a shower with a larger number of elements. This recombination is performed in step 4.

Step 3 — Validation against IAU MDC

The groupings that are considered potential showers are validated against the showers currently found in the MDC list. This validation is done by performing the D test between the average orbit of each grouping and the orbital parameters of each of the showers in the MDC list. The average orbit is calculated as the arithmetic mean of the orbital elements of the meteors of the same grouping.

If the result of the D test is greater than D_{maxiau} (the study considered $D_{maxiau} = 0.22$. This value represents a safe margin to say that the orbits of the two showers are different enough to be considered two different showers), the grouping is considered a new shower candidate.

If the result of the D test is lower than D_{maxiau}, other parameters such as solar longitude, RA, DEC, and geocentric velocity are tested. If these parameters differ by a large amount (like 30–40%), the result is also considered a new shower candidate, otherwise the grouping is discarded. This is an interesting test since there may be showers with the same orbital characteristics, but with different other parameters (like solar longitude in Eta Aquariids and Orionids).

Step 4 — Refinement and Confirmation

The first 3 steps can be performed automatically, i.e., no manual steps are necessary. The output of the third step is a list of candidate groupings for new showers. In step 4, each of these candidates is manually tested in an attempt to find all the orbits that belong to the shower, an attempt is also made to find the best average orbit, i.e., the location of the largest concentration of orbits of the shower (the center of the shower). This method was named "Lapdeitor".

It has 3 parameters: Initial average orbit, D_{maxl}, and N, which represents the number of iterations desired. The algorithm executes N iterations, and each iteration searches the database for orbits distant less than D_{maxl} from the average input orbit (in the first interaction the initial average orbit is used). The orbits that are found are added to a list, and a new average orbit is calculated from the mean of the orbits of that list. This new average orbit is then used as the input orbit of the next iteration.

If the orbits are concentrated near the average orbit, at each iteration more orbits near the center are returned in the search, thus increasingly influencing the calculation of the average orbit. As a consequence, the average orbit will tend to migrate gradually towards the average orbit representing the shower center.

At the end of N iterations, the average orbit tends to be closer to the highest concentration of orbits of the shower. Figure 3 graphically depicts the behavior of the data returned at each iteration of the algorithm. The plot symbolically represents the concentration of orbits around the shower center, in relation to the D value.

The N value must be large enough so that interactions $N - 1$ and N have the same result.

The D_{maxl} value must be chosen carefully. Exceedingly high values might return false centers, especially

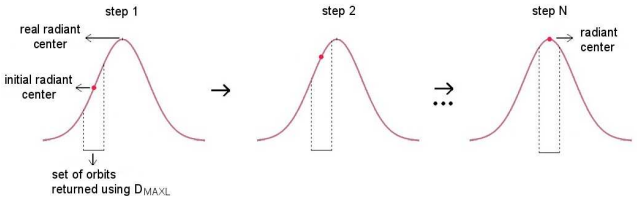

Figure 3 – Representation of steps 1 to N of Lapdeitor.

if the average orbit is close to two centers. A graphical representation of this behavior is shown in Figure 4.

Large D_{maxl} values may also prevent small centers from being found. This can happen if two centers are close to each other and one is much larger than the other. On the other hand, exceedingly small values can prevent the convergence of the average orbit to the nearest center.

The distribution of shower orbits does not always follow the same pattern. Some showers have well concentrated orbits and others are more sparse. Thus, the D_{maxl} parameter must be chosen according to the characteristics of the shower. The Break-point+ and Valideitor methods (which will be presented in Step 5) can help to understand the characteristics of each shower and so help to choose a suitable value for the D_{maxl}.

To minimize problems, Lapdeitor must be run multiple times, and at each time smaller values of D_{maxl} should be used. By doing that it is possible to find the center of a shower more accurately.

During the execution of Lapdeitor, it is possible to generate an XY graph, in which the X axis corresponds to the current iteration and the Y axis corresponds to the number of orbits found from the list of orbits using the D_{maxl} value in the search.

After finding the probable center of the shower, it is necessary to perform a new verification in order to validate if the orbits of the center actually belong to a shower. The test verifies if the shower center is represented by at least 6 orbits. It also tests the center's average orbit against the existing showers in the MDC database. This need arises from the fact that the average orbit of the center may now be displaced relative to the initial average orbit of the shower, which had al-

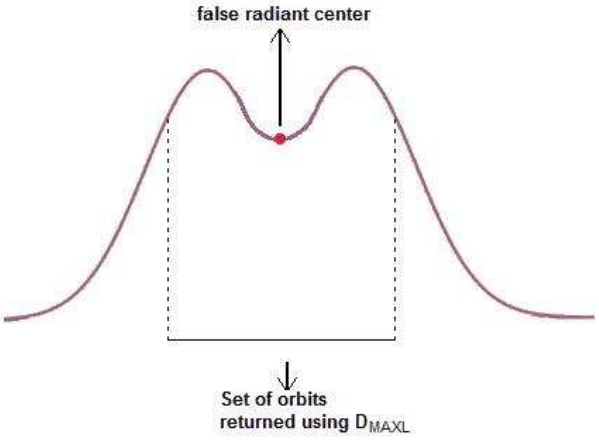

Figure 4 – False center returned when D_{maxl} is too large.

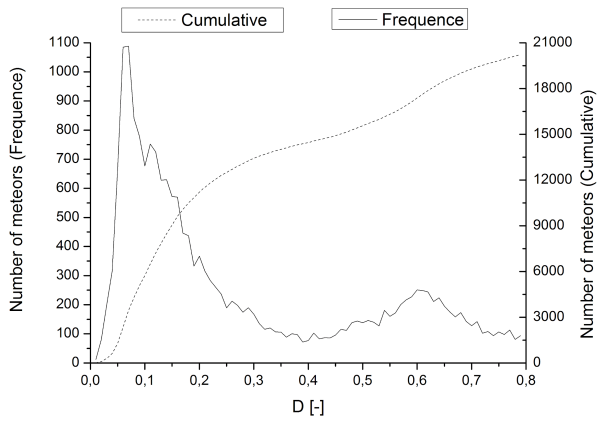

Figure 5 – Southern Taurids Break-point.

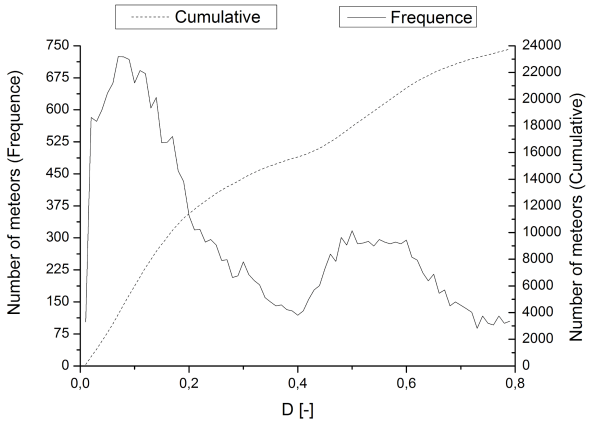

Figure 6 – Southern Taurids* Break-point.

ready been checked against the IAU list in step 3. Each shower that passes the tests can then be considered a new shower.

In order to demonstrate the use of Lapdeitor, all steps of the process were executed for the Southern Taurids shower. Table 1 shows the results of Lapdeitor for this shower. The last MDC report was used as initial orbit in Lapdeitor, and the result was the average orbit of Southern Taurids*. Figures 5 and 6 show the break-point (Welch, 2001; Neslušan et al., 2013) plots using the D criterion for both average orbits (Step= 0.01). It is possible to see that the Southern Taurids* plot (to the right) has a steeper slope at low D. This indicates that it is closer to the actual center of the shower. It is also possible to see that Southern Taurids* encompasses more orbits in total.

Step 5 — Shower Characteristics and Final Validation

At the end of the fourth step, a set of new showers is found, each representing a concentration of orbits around an average orbit. It is also known that the average orbit is far from showers known by the MDC. These characteristics alone would be enough to confirm a new shower, however, to exercise caution, it is necessary to understand how the shower's orbits are distributed and what their relation with nearby showers is.

Following that, new showers can be submitted to new methods that aid in understanding and validating their characteristics. The first method is a break-point variation. The second is a totally new method, called Valideitor, both being related and complementary to each other. In addition, the shower orbits can be represented in 3D, thus dismissing any uncertainties that may still persist.

Break-point+

The break-point implementation uses as its input the orbital values of a shower in addition to the following parameters: $D_{initial}$, D_{final}, $D_{current}$ and Step. The algorithm executes a number of iterations, and in the first iteration the value of $D_{current}$ is equal to $D_{initial}$, and at the end of each iteration the Step value is added to $D_{current}$. This process is repeated until $D_{current}$ becomes larger than D_{final}.

In each iteration, the algorithm goes through the list of orbits from the catalogs searching for orbits whose D test value between itself and the orbital values of the input shower is lower than or equal to $D_{current}$. The number of orbits that satisfy this parameter is then added to a linear plot. This result is shown by the dotted lines in Figure 5.

A second line is also implemented (it is represented by the solid lines in Figure 5). This line represents the change in the number of orbits in an iteration relative to the previous iteration.

In Figure 7 we can see that the inflection point of the dotted lines is approximately at $X = 0.2$, this is the break-point. We can also see that after the break-point, even for large values of X, few orbits are added to the dotted line, which shows that the orbits of the shower are concentrated near its average orbit (the more concentrated, the lower the break-point).

However, the break-point method has problems when analyzing a shower that has other showers nearby, in the sense of orbital proximity. This problem is further aggravated if one of the nearby showers is much larger than the shower being tested, in such cases, the plot may show several inflection points or none at all.

To minimize this problem, the break-point+ method is proposed. In this method the orbits used in the break-point are filtered out. This filter uses the RA/DEC coordinates of the shower as the center point, and a spherical cap with radius equal to R is drawn. Only those orbits whose RA/DEC fall inside the cap area shall be considered in the break-point. We can see in

Table 1 – Southern Taurids Result.

Name	Solar Longitude	RA	DEC	V_g	a	q	e	ω	Ω	i
Southern Taurids	211.3	42.8	10.6	27.0	1.85	0.368	0.807	114.8	31.3	5.4
Southern Taurids*	221.01	52.72	15.36	27.92	2.02	0.354	0.822	115.09	41.01	5.26

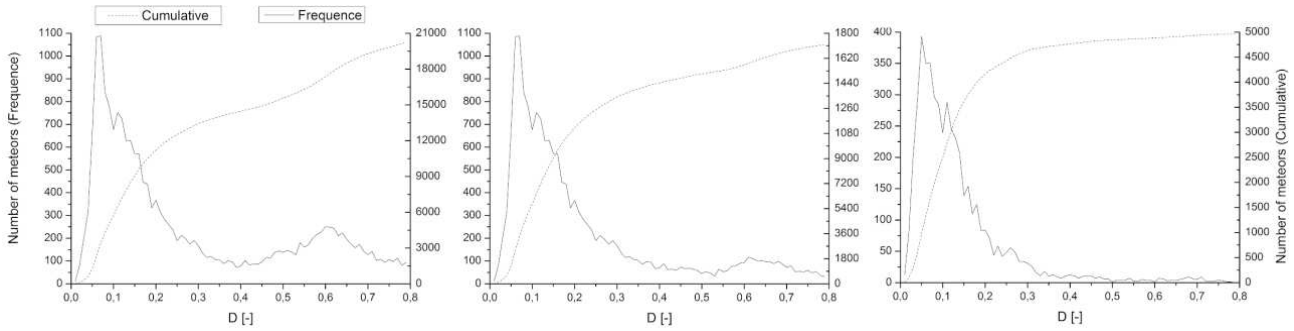

Figure 7 – Variation of the R parameter in the Break-point+ of the Southern Taurids shower. From left to right: $R = 360$, 50 and 10 degrees were used.

Figure 7 how the variation of the R parameter impacts the result of break-point+.

The break-point plot with $R = 10$ degrees shows a clearer picture (with fewer inflection points in the plot), making it easier to understand the distribution of orbits in relation to the average orbit. This happens because the filter eliminates showers that are too distant (in RA/DEC) to the average orbit of the shower being analyzed. The R value can be different for each shower. It must be chosen so that only a few shower's orbits are missed, while also limiting the influence of other showers. The R parameter also must be chosen with a value large enough to accommodate the drift of the radiant.

Valideitor

In order to better understand the relation between a shower and other showers close to it (in the orbital and chronological sense), a new method was proposed. This method is called Valideitor and it was designed to analyze, over time (day to day), the number of orbits that belong to a given shower. To determine if an orbit belongs to a shower, the D test is performed between this orbit and the average orbit of the shower. If the result is lower than a given D_{maxv}, usually the break-point value or a value close to 0.21, the orbit is considered as belonging to the shower.

Over time, and as the shower's peak approaches, the number of orbits that fit to the shower tends to increase, and therefore a peak can be seen in the plot.

To prevent the plot from growing indefinitely, a reduction factor is applied, thus, after the shower's peak date, the number of orbits tends to decrease and the plot tends to a minimum.

With this method it is possible to see the distribution of the orbits over time, and also how these orbits fit to the shower.

The method also allows us to understand the distribution of orbits that are near the shower, but that do not fit into it. This provides a better understanding of the characteristics of the shower and its neighborhood. As an example, Figure 8 shows the result of Valideitor for the Geminids shower. In this figure, a radius of 10 degrees with respect to the shower center was analyzed. We can see that the shower's peak is concentrated, and it stands out among the orbits that do not belong to the shower.

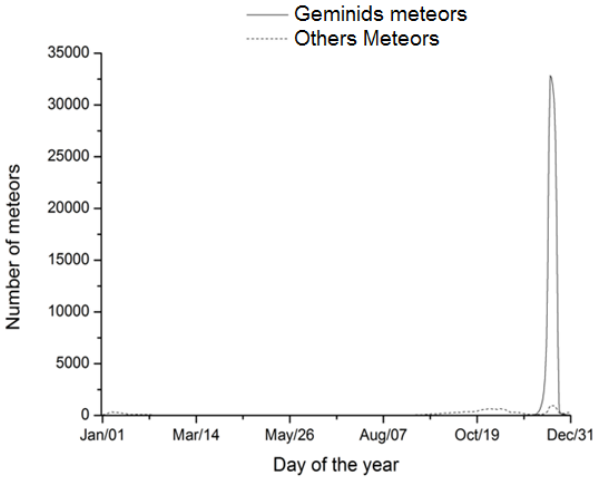

Figure 8 – Valideitor of the Geminids Shower. The X axis represents the days of the year and the Y axis represents the number of orbits. The solid line represents the orbits that fit the shower ($D_{maxv} = 0.21$ was used), and the dashed line represents the orbits that did not fit the shower.

In the implementation of this method the same RA/DEC filter described in the Break-point+ method was used, and the following parameters were provided as input: D_{maxv}, InitialDate, FinalDate, CurrentDate, and DateDelta.

The method consists of executing a number of iterations. In the first iteration, the CurrentDate parameter is set to InitialDate, and at the end of each iteration the current date is incremented by one day (this parameter can be changed). The iterations continue until CurrentDate is equal to FinalDate. At each iteration the following steps are performed: (i) A list called CurrentList is created. This list includes all the orbits whose dates have the same day/month as the CurrentDate (disregarding the year), (ii) A D test is performed between each of the orbits in the CurrentList and the shower's orbit. If the result of the D test is lower than D_{maxv}, the orbit is added to a new list called ShowerList; (iii) A point is added to the plot corresponding to the number of orbits currently in the ShowerList. This point represents the number of orbits that belong to the Shower; (iv) Another point is added to the plot corresponding to the number of elements in the CurrentList less the number of elements in the ShowerList. This point represents the number of orbits that do not belong to the

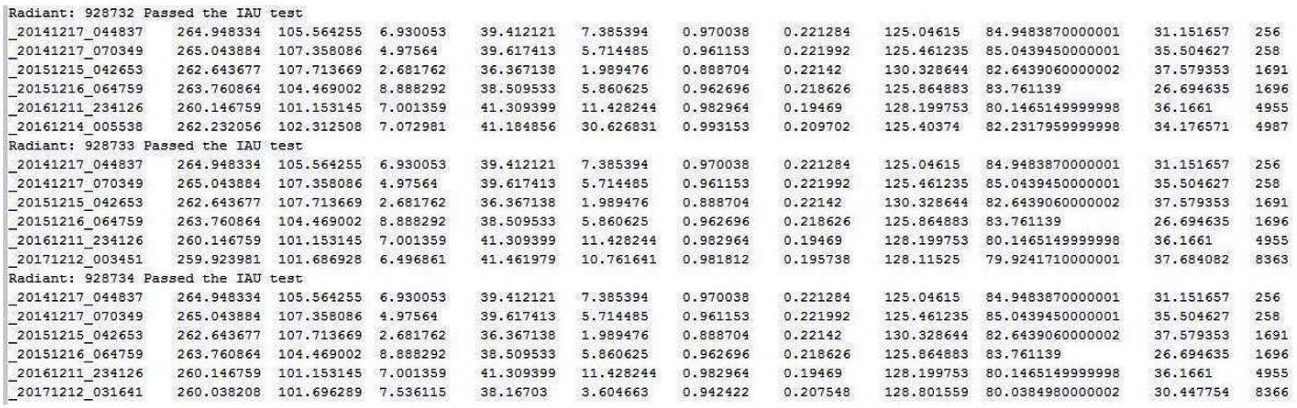

Radiant: 928732 Passed the IAU test											
_20141217_044837	264.948334	105.564255	6.930053	39.412121	7.385394	0.970038	0.221284	125.04615	84.9483870000001	31.151657	256
_20141217_070349	265.043884	107.358086	4.97564	39.617413	5.714485	0.961153	0.221992	125.461235	85.0439450000001	35.504627	258
_20151215_042653	262.643677	107.713669	2.681762	36.367138	1.989476	0.888704	0.22142	130.328644	82.6439060000002	37.579353	1691
_20151216_064759	263.760864	104.469002	8.888292	38.509533	5.860625	0.962696	0.218626	125.864883	83.761139	26.694635	1696
_20161211_234126	260.146759	101.153145	7.001359	41.309399	11.428244	0.982964	0.19469	128.199753	80.1465149999998	36.1661	4955
_20161214_005538	262.232056	102.312508	7.072981	41.184856	30.626831	0.993153	0.209702	125.40374	82.2317959999998	34.176571	4987
Radiant: 928733 Passed the IAU test											
_20141217_044837	264.948334	105.564255	6.930053	39.412121	7.385394	0.970038	0.221284	125.04615	84.9483870000001	31.151657	256
_20141217_070349	265.043884	107.358086	4.97564	39.617413	5.714485	0.961153	0.221992	125.461235	85.0439450000001	35.504627	258
_20151215_042653	262.643677	107.713669	2.681762	36.367138	1.989476	0.888704	0.22142	130.328644	82.6439060000002	37.579353	1691
_20151216_064759	263.760864	104.469002	8.888292	38.509533	5.860625	0.962696	0.218626	125.864883	83.761139	26.694635	1696
_20161211_234126	260.146759	101.153145	7.001359	41.309399	11.428244	0.982964	0.19469	128.199753	80.1465149999998	36.1661	4955
_20171212_003451	259.923981	101.686928	6.496861	41.461979	10.761641	0.981812	0.195738	128.11525	79.9241710000001	37.684082	8363
Radiant: 928734 Passed the IAU test											
_20141217_044837	264.948334	105.564255	6.930053	39.412121	7.385394	0.970038	0.221284	125.04615	84.9483870000001	31.151657	256
_20141217_070349	265.043884	107.358086	4.97564	39.617413	5.714485	0.961153	0.221992	125.461235	85.0439450000001	35.504627	258
_20151215_042653	262.643677	107.713669	2.681762	36.367138	1.989476	0.888704	0.22142	130.328644	82.6439060000002	37.579353	1691
_20151216_064759	263.760864	104.469002	8.888292	38.509533	5.860625	0.962696	0.218626	125.864883	83.761139	26.694635	1696
_20161211_234126	260.146759	101.153145	7.001359	41.309399	11.428244	0.982964	0.19469	128.199753	80.1465149999998	36.1661	4955
_20171212_031641	260.038208	101.696289	7.536115	38.16703	3.604663	0.942422	0.207548	128.801559	80.0384980000002	30.447754	8366

Figure 9 – Output from step 3. The lines of the orbits are represented by the parameters: orbit capture date, solar longitude, RA, DEC, V_g, a, e, q, ω, Ω, i and line of the input file.

Shower; and (v) All orbits whose capture date is earlier than CurrentDate minus DateDelta are removed from the ShowerList. This is the plot's reduction mechanism. DateDelta must be proportional to the duration of the shower. Values between 7 and 15 days were used for this parameter in the tests performed.

Search for Parent Bodies

The last task of step 5 is trying to find the parent body or bodies that created the shower. For that, a simple method to search for the parent body is executed, using as its input the orbital parameters and the D_{maxp} parameter. The algorithm reads the orbital parameters from a file provided by the Jet Propulsion Laboratory (JPL, 2018), which has hundreds of thousands of orbits of celestial bodies in the solar system, and performs a D test between these orbits and the input orbit.

The search returns all records in the JPL file for which the D test is lower than D_{maxp}. With this result, retroactive simulations are performed in order to validate if these elements belong to the parent body of the shower.

3 Application of the Method

To demonstrate the new method, a test was performed through which an existing shower was rediscovered, more precisely the December Monocerotids (MON) shower, whose orbital elements were intentionally removed from the MDC list used in step 3.

Step 1 was executed using the BRAMON database (with 6 805 orbits). In this step, 106 clusters were found using the parameters $D_{maxc} = 0.07$, minPoints= 5, and ClusterSize= 6. Step 2 was executed using the parameters ClusterSizeMax= 35, ShowerMin= 6, and $D_{maxa} = 0.07$. As a result, 1 394 534 combinations of 6 orbits were found that meet the criteria that characterize a shower. These combinations were then validated against the MDC database using $D_{maxiau} = 0.22$ and 132 combinations were found as candidates of new showers. Analyzing these 132 combinations, 125 corresponded to groups that fit the expected orbit of the MON shower. In Figure 9 three of these groups of orbits are shown.

Table 2 lists the average orbit generated from the first group (928732 in Figure 9).

By executing step 4, the average orbit can be refined using Lapdeitor with $D_{maxl} = 0.07$, and the BRAMON, SonotaCo, and EDMON databases. Line 1 of Table 3 lists a new average orbit found by this method, which closely resembles the known orbit of the MON shower published in the last MDC report (line 2 of Table 3).

By performing a search for all records distant up to D = 0.05 from the new orbit and from the MON shower, it was shown that a search using the new orbit returns more elements than the current MON orbit, 800 compared to 782. In other words, the method not only rediscovered the shower, but it also managed to define an orbit that is closer to the center of the shower.

4 Conclusions

Over a short period of time the new shower search method has demonstrated its strong capability to find new showers. Until the present date, this method has been responsible for the discovery of 121 new showers, that have already been submitted to the Meteor Data Center (in *pro tempore*). The presentation and detailing of these new showers will be carried out in a next article. This represents more than 12% of all showers ever discovered. The method is capable of finding and improving large previously known showers, but it stands out in the search for small showers.

After decades of continuous searches for new showers, most of the large showers have already been identified and published. Currently, the search is focused on small showers and on showers that come from the same region of the sky as other previously discovered showers. Visual identification methods may not be able to identify such showers, however, this new search method uses orbital data, and is thus capable of identifying showers in these scenarios.

The new method uses orbital data, clustering algorithms, combinatorial analysis, validation against the MDC database, mechanisms of refinement and validation of showers, as well as resources to search for possible parent bodies. It is also able to perform the search for new showers by simultaneously using the capture

Table 2 – Average orbit of the group (928732). The parameter values were rounded in order to accommodate the table.

Name	$\lambda_\odot$	RA	DEC	V_g	a	q	e	ω	Ω	i	Line
_20141217_044837	264.9483	105.6	6.9	39.41	7.39	0.2213	0.9700	125.046	84.948	31.15	256
_20141217_070349	265.0439	107.4	5.0	39.62	5.71	0.2220	0.9612	125.461	85.044	35.50	258
_20151215_042653	262.6437	107.7	2.7	36.37	1.99	0.2214	0.8887	130.329	82.644	37.58	1691
_20151216_064759	263.7609	104.5	8.9	38.51	5.86	0.2186	0.9627	125.865	83.761	26.69	1696
_20161211_234126	260.1468	101.2	7.0	41.31	11.43	0.1947	0.9830	128.200	80.147	36.17	4955
_20161214_005538	262.2321	102.3	7.1	41.18	30.63	0.2097	0.9932	125.404	82.232	34.18	4987
Average:	263.1293	104.8	6.3	39.40	10.50	0.2146	0.9598	126.717	83.129	33.55	—

Table 3 – Average orbit after Lapdeitor (using the BRAMON, EDMOND, and SonotaCo databases).

Radiant	$\lambda_\odot$	RA	DEC	V_g	a	q	e	ω	Ω	i
Radiant Found	258.72	101.17	8.7	40.9	15.03	0.189	0.977	129.3	78.7	34.7
MON	258.5	100.5	7.9	41.5	13.4	0.19	0.985	128.9	78.5	35.8

databases of several meteor video-monitoring networks.

In addition to the search for new showers, the method also offers two mechanisms that help to improve the understanding of showers, Valideitor and BreakPoint+. These new mechanisms provide important data to better understand the showers and how they relate to each other. The combination of these mechanisms and the possibilities they offer make the new method unique and capable of boosting the study of showers.

References

Amaral L., Trindade L., Di Pietro C., Zurita M., Poltronieri R., Silva G., Jacques C., Jung C., and Koukal J. (2017). "Brazilian Meteor Observation Network: History of creation and first developments". In *Proceedings of the International Meteor Conference, Petnica, Serbia, September 21-24 2017*. International Meteor Organization.

Ceplecha Z., Borovička J., Elford W. G., Revelle D. O., Hawkes R. L., Porubčan V., and Šimek M. (1998). "Meteor phenomena and bodies". *Space Science Reviews*, **84**, 327–471.

Drummond J. D. (1981). "A test of comet and meteor shower associations". *Icarus*, **45**, 545–553.

EDMOND (2018). "EDMOND Database". `http://www.daa.fmph.uniba.sk/edmond` .

Ester M., Kriegel H.-P., Sander J., and Xu X. (1996). "A density-based algorithm for discovering clusters in large spatial databases with noise". In *Proceedings of the Second International Conference on Knowledge Discovery and Data Mining (KDD-96)*. AAAI Press, pages 226–231.

Galligan D. P. (2001). "Performance of the D-criteria in recovery of meteoroid stream orbits in a radar data set". *Mon. Not. R. Astro. Soc.*, **327**, 623–628.

Jopek T. J., Valsecchi G. B., and Froeschlé C. (2002). "'Asteroid meteoroid streams'". In Bottke W. F., Cellino A., Paolicchi P., and Binzel R. P., editors, *Asteroids III*, Tucson. Univ. Arizona Press, pages 645–652.

JPL (2018). "Jet Propulsion Laboratory". `https://www.jpl.nasa.gov/` .

Kornoš L., Koukal J., Piffl R., and Tóth J. (2014a). "EDMOND Meteor Database". In Gyssens M., Roggemans P., and Zoladek P., editors, *Proceedings of the International Meteor Conference, Poznań, Poland, Aug. 22-25, 2013*. International Meteor Organization, pages 23–25.

Kornoš L., Matlovič P., Rudawska R., Tóth J., Hajduková, Jr. M., Koukal J., and Piffl R. (2014b). "Confirmation and characterization of IAU temporary meteor showers in EDMOND database". In Jopek T. J., Rietmeijer F. J. M., Watanabe J., and Williams I. P., editors, *Proceedings of the Meteoroids 2013 Conference, A.M. University, Poznań, Poland, Aug. 26-30, 2013*. pages 225–233.

MDC (2018). "IAU Meteor Data Center". `https://www.ta3.sk/IAUC22DB/MDC2007/` .

Neslušan L., Svoreň J., and Porubčan V. (2013). "The method of selection of major-shower meteors revisited". *Earth, Moon, and Planets*, **110**, 41–66.

SonotaCo (2009). "A meteor shower catalog based on video observations in 2007–2008". *WGN, Journal of the IMO*, **37**, 55–62.

SonotaCo (2018). "SonotaCo Network Simultaneously Observed Meteor Data Sets". `http://sonotaco.jp/doc/SNM/` .

Southworth R. B. and Hawkins G. S. (1963). "Statistics of meteor streams". *Smithsonian Contributions to Astrophysics*, **7**, 261.

Sugar G., Moorhead A., Brown P., and Cooke W. (2017). "Meteor shower detection with density-based clustering". *Meteoritics & Planetary Science*, **52:6**, 1048–1059.

Welch P. G. (2001). "A new search method for streams in meteor data bases and its application". *Mon. Not. R. Astron. Soc.*, **328**, 101–111.

Handling Editor: Željko Andreić

Radio meteors

Forward Scattering : an interesting formula to calculate the velocity of a meteoroid that generates a head echo

Pierre Ernotte [1]

In this article, we show that the velocity of a meteoroid that generates a "head echo" depends only on the slope of the Doppler variation curve and on the value of half of the first Fresnel zone. We also show that the formula obtained is consistent with formulas given by Richardson J. (1998).

Received 2018 September 28

1 Introduction

In this figure, there is a sudden change in the frequency at the front of the echo.

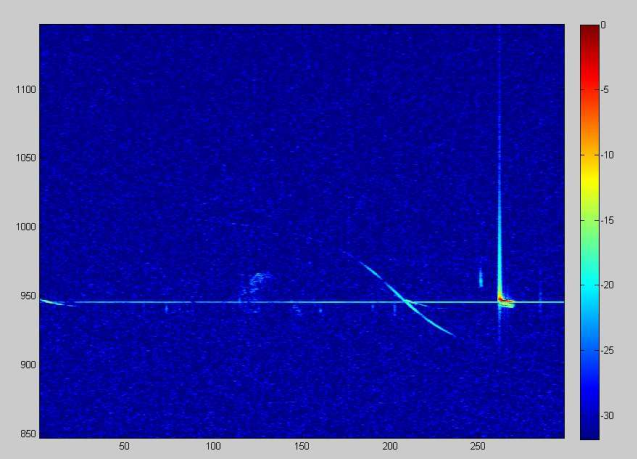

Figure 1 – An example of spectrum analysis of a head echo (frequency versus time)

A zoom on the spectrogram shows the linear frequency variation at the front of the echo.

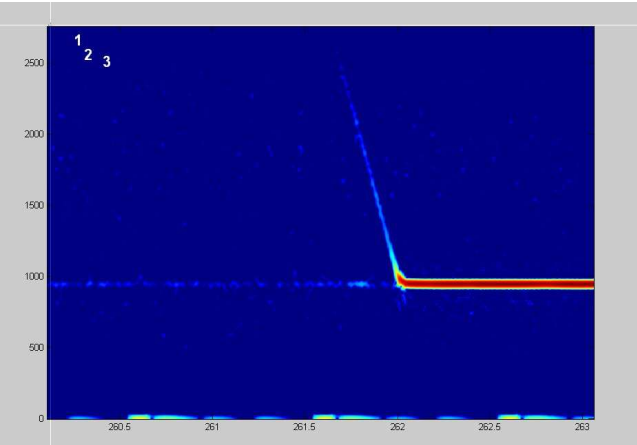

Figure 2 – A zoom on the same head echo spectrum as in Figure 1.

We present an amazing formula that is useful to calculate the velocity of the corresponding meteoroid.

[1]Email: ernotp@gmail.com

IMO bibcode WGN-466-ernotte-velocity
NASA-ADS bibcode 2018JIMO...46..198E

2 Calculating the velocity

In his article Chris Steyaert (2010) gives the formulas of the Doppler shift and his first derivative. The latter being measurable on the spectrogram, the idea is to use it to calculate the velocity of the head echo.

The geometry of the problem is the following McKinley (1961, p. 238):

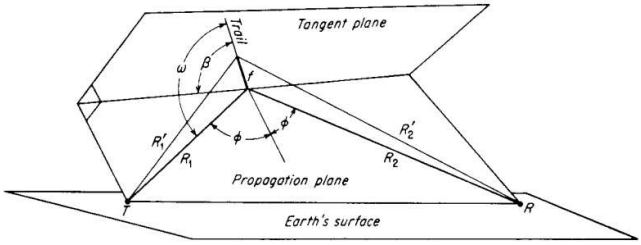

Figure 3 – The geometry of forward scattering.

T is the transmitter, R the receiver and M is the point of specular reflection. The trail is tangent to an ellipsoid which T and R are the foci. ω is the angle between the trail and TM and and ω' is the angle between the trail and RM. β is the angle between the trajectory and the plane of propagation. φ is half of the angle at which the point of specular reflection sees the transmitter-receiver segment. Following McKinley, ω' is the supplement of ω.

The Doppler shift formulas provided by Steyaert (2010) are: $Doppler_T = -\frac{\overrightarrow{TM}}{|\overrightarrow{TM}|}.\overrightarrow{v}\frac{f}{c} = \frac{v}{c}f\cos\omega$ is the Doppler shift from the transmitter to the meteor. $Doppler_R = -\frac{\overrightarrow{RM}}{|\overrightarrow{RM}|}.\overrightarrow{v}\frac{f}{c} = \frac{v}{c}f\cos\omega'$ is the Doppler shift from the meteor to the receiver. Since the point M is the point of specular reflection, we have $\omega' = \pi - \omega$ at this point. We can see that the total Doppler shift is zero at the point of specular reflection, which is normal.

The formulas (15) and (16) of Steyaert (2010) for calculating the derivative of the total Doppler shift are:

3.2 Doppler shift derivative

Similar to the Doppler shift itself, the derivative or slope of the Doppler shift for receiver 'i' is the sum of two parts:

$$\frac{\partial Doppl_i}{\partial t} = \frac{\partial Doppl_T}{\partial t} + \frac{\partial Doppl_{R_I}}{\partial t} \tag{14}$$

Assuming a time independent velocity vector $\overline{v}$

$$\frac{\partial Doppl_T(t)}{\partial t} = -\frac{1}{\left|\overline{TM}\right|}\left[v^2 - \frac{\left(\overline{TM}\cdot\overline{v}\right)^2}{TM^2}\right]\frac{f}{c} \tag{15}$$

$$\frac{\partial DopplR_i(t)}{\partial t} = -\frac{1}{\left|\overline{R_iM}\right|}\left[v^2 - \frac{\left(\overline{R_iM}\cdot\overline{v}\right)^2}{R_iM^2}\right]\frac{f}{c} \tag{16}$$

They become:

$$-\frac{\partial Doppler_{total}}{\partial t} = \frac{f}{c}\left(\frac{v^2}{TM} - \frac{v^2\cos^2\omega}{TM} + \frac{v^2}{RM} - \frac{v^2\cos^2\omega'}{RM}\right)$$

As $\cos\omega = \sin\varphi\cos\beta$ and $\omega' = \pi - \omega$ at the point M (see McKinley (1961, p. 238)), we have:

$$-\frac{\partial Doppler_{total}}{\partial t} = \frac{f}{c}\left(\frac{1}{TM} + \frac{1}{RM}\right)\left(v^2 - v^2\sin^2\varphi\cos^2\beta\right)$$

One can deduce the velocity v from this formula:

$$v^2 = -\frac{\partial Doppler_{total}}{\partial t}\left(\frac{TM.RM}{TM+RM}\right)\left(\frac{1}{1-\sin^2\varphi\cos^2\beta}\right)\frac{c}{f}$$

There is an amazing relationship:
According to McKinley (1961), half of the first Fresnel zone which we will call MM1 is expressed as follows:

$$MM1 = \sqrt{\lambda\frac{TM.RM}{TM+RM}\cdot\frac{1}{(1-\sin\varphi^2\cos^2\beta)}}$$

As $\lambda = \frac{c}{f}$

$$\boxed{v = MM1\sqrt{-\frac{\partial Doppler_{total}}{\partial t}}} \tag{1}$$

We have shown that the velocity of the meteoroid depends only on the slope of the Doppler shift and the value of half of the first Fresnel zone.

3 Special cases

3.1 The trail is in the propagation plane

If the trail is in the propagation plane, then $\cos\beta = 1$. Felix Verbelen demonstrated that MM1 can be calculated if the height of ionization of the meteoroid and the elevation of the trail are known and if its orbit is in the vertical plane passing through the beacon and the receiver. We can estimate that the height is between 85 km and 110 km. The elevation of the trail is known in the case of stream meteor: it is the elevation of its radiant. So, in this case, the velocity v is completely determined.

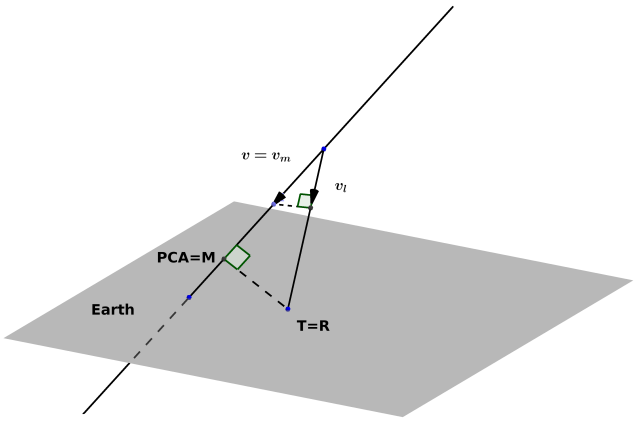

Figure 4 – The geometry of back scattering.

3.2 Backscattering

In the case of backscattering, we have: $TM = RM$ and $\varphi = 0$. We have the following situation:

The previous relation for the calculation of MM_1 becomes:

$$MM1 = \sqrt{\lambda\frac{TM}{2}}$$

and we know that:

$$v = MM1\sqrt{-\frac{\partial Doppler_{total}}{\partial t}}$$

This formula can be deduced from a relationship provided by Richardson (1998).

$$\Delta f = -sign(\Delta t)\sqrt{\left(\frac{2f_0}{c}\right)^2\frac{v_m^2}{\frac{r_0^2}{v_m^2\Delta t^2}+1}}$$

that becomes:

$$\Delta f = -sign(\Delta t)\sqrt{\left(\frac{2f}{c}\right)^2\frac{v^2}{\frac{TM^2}{v^2\Delta t^2}+1}}$$

With $\frac{\Delta f}{\Delta t} = \frac{\partial Doppler_{total}}{\partial t}$

For $\Delta t \ll$, the general equation is simplified because the factor 1 of the denominator becomes negligible.

$$\Delta f = -sign(\Delta t)\sqrt{\left(\frac{2f}{c}\right)^2\frac{v^2}{\frac{TM^2}{v^2\Delta t^2}}}$$

Thus:

$$\Delta f \simeq -\frac{2fv^2}{cTM}\Delta t$$

thus

$$v = \sqrt{-\frac{c}{f}\frac{TM}{2}\frac{\Delta f}{\Delta t}}$$

The relationship

$$v = \sqrt{-\lambda \frac{TM}{2} \frac{\partial Doppler_{total}}{\partial t}}$$

is identical to the relationship stated above since

$$MM1 = \sqrt{\lambda \frac{TM}{2}}$$

Acknowledgments

We wish to thank Felix Verbelen for very helpful discussions.

References

McKinley D. W. R. (1961). *Meteor Science and Engineering*. McGraw-Hill. page 238.

Richardson J. and Kuneth W. (1998). "Revisiting the Radio Doppler Effect from Forward-scatter Meteor Head Echoes". *WGN, Journal of the IMO*, **26:3**, 121.

Steyaert C., Verbelen F., and de VVS Beacon Observers (2010). "Meteor Trajectory from Multiple Station Head Echo Doppler Observations". *WGN, Journal of the IMO*, **38:4**, 123–129.

Handling Editor: Jean-Louis Rault
This paper has been typeset from a LaTeX file prepared by the author.

Visualizing sporadic meteor radiants and their dynamics by radio forward scattering

Wolfgang Kaufmann[1]

Frequency gradients of forward scattered head echoes are used to distinguish between different sources of sporadic meteors. This approach requires a basic radio station only. By means of kernel density mapping the antihelion, apex and helion source could be displayed as well as their dynamic composition of different radiants in time and space during a continuous 40 day measuring campaign. The study of the dynamics was performed with a 10 day as well as a daily resolution.

Received 2018 September 5

1 Introduction

Sporadic meteors are considered as meteors not being part of a recognized shower. The distribution of the radiants of sporadic meteors within the celestial sphere were subject of a number of surveys. Since 1959 it is known that the sources of sporadic meteors are non-homogeneously distributed in space (Hawkins, 1956). Jones and Brown (1993) identified 6 regions with increased activity: north and south toroidal source, antihelion (AH) and helion (H) source and north and south apex (AP). Seasonal variations also were studied and revealed the dynamics of the single sources throughout the year (Campell-Brown & Jones, 2006; Campell-Brown & Wiegert, 2009). The effect of the visibility of the sources in dependence of latitude and season of year on the observed meteor count rates was investigated by Younger et al. (2009).

For the meteor amateur astronomer as an individual such studies are not easily to accomplish. An optical observation delivers concrete directional parameters of observed meteors but is restricted to night time and clear skies. A basic meteor radio station in standard mode provides no directional information but can be used for observation 24 hours a day. This paper describes a qualitative approach to study the dynamics of sporadic meteor occurrence based on radio forward scatter. Only prerequisite is a radio meteor receiving and detecting system that is able to pick up the frequency change of meteor head echoes with a sufficient time and frequency resolution.

Utilising meteor head echoes can provide directional information. The frequency of radio waves scattered at the plasma sheet surrounding the meteoroid during its flight through the terrestrial atmosphere (Close et al., 2002) is continuously altering. This is a result of the changing radial velocities of the meteoroid with respect to the observer and to the transmitter, as well as its deceleration during its flight. Different radial velocity changes generate different frequency gradients as long as the scattering originates from a circumscribed fixed region. They attribute to meteoroids of different origin in terms of altitude, azimuth and geocentric velocity. Because the meteoroid-receiver geometry is unknown a concrete position in the celestial sphere cannot be calculated from the frequency gradients. However a statistical method, the Kernel Density Map (KDM), can make visible the distribution of the frequency gradients of meteor head echoes thereby indicating different radiants (Kaufmann, 2018). The closer and more numerous the frequency gradients cluster at different positions in a frequency gradient vs. time diagram the higher the calculated local density (via a kernel function) will be. This local density is displayed by a shade of grey in the KDM. Thus a hot spot means there is a bunch of meteors having very similar frequency slopes at a certain time. This basically can be ascribed to a common origin in space, i.e. this bunch of meteors is an indication for a (micro)shower.

By this technique the dynamics of emerging and disappearing of micro showers and the fluctuation of activity within the broad persistent sporadic meteor sources can be studied at least qualitatively. The results of a measuring campaign from January to February 2018 are presented.

2 Material and Methods

The French radar-transmitter GRAVES was employed for forward scattering. It transmits a continuous rf-signal at a frequency of 143.050 MHz and illuminates a well defined region of the sky in 100 km height over southern France. Receiving location was Algermissen, Northern Germany (N 52°15′.16, E 009°58′.71). A HB9CV antenna was directed to the transmitter location and fed to a FUNcube Dongle Pro+ (FCDP). The FCDP is a software defined receiver[a]. This means all filtering and demodulation is done by software. SDR# was used as receiving software[b]. It was set to USB, 143.049 MHz receiving frequency, 48 kHz audio output, audio filtering and AGC switched off. The audio output was fed to the software Meteor Logger[c], which detects and logs meteor signals within an audio stream (Kaufmann, 2017). It reveals a continuous output i.a. of the frequency of the detected signal in 10.7 ms steps. Both programs ran on the same computer (Intel i5, clock speed 2.3 GHz) with Windows 7. Observation period was 2018 January 5 to February 17.

The software Process Data[c] was used to edit the gathered raw data. It filtered out interference, merged intermitted meteor signals, identified the head echoes

[1]Lindenweg 1e, 31191 Algermissen, Germany.
Email: contact@ars-electromagnetica.de

IMO bibcode WGN-466-kaufmann-vizualizing
NASA-ADS bibcode 2018JIMO...46..201K

[a]http://www.funcubedongle.com/
[b]https://airspy.com/download/
[c]http://www.ars-electromagnetica.de/robs/download.html

Table 1 – Main issues of the observation period 2018 January 5, 17^h UTC to February 17, 16^h59^m UTC.

Observing Time [h]	Total Counts	Head Echo Counts	% Head Echoes	Mean Head Echoes/h
1030	34280	3443	10.04 %	3.3

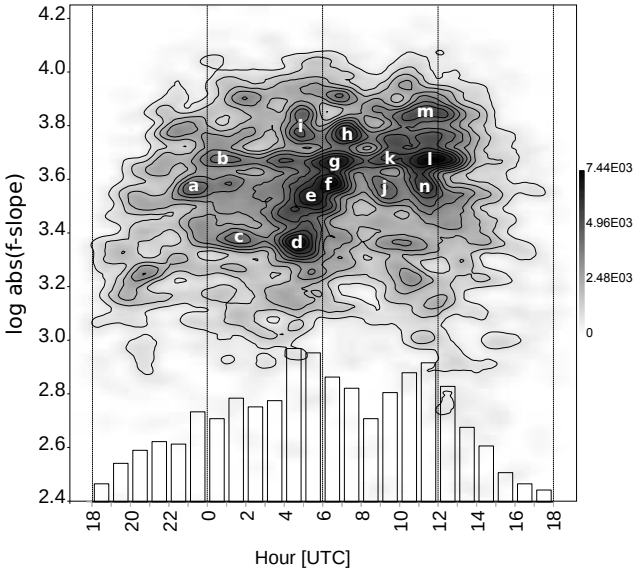

Figure 1 – Kernel density map of the frequency slopes of head echoes from 40 × 24 h of continuous observation (Jan 5 – Feb 14). The cumulated head echo counts per hour are added as bar chart (Maximum 247 Head echoes/h). Daily time span is $18^h - 17^h59^m$ UTC. The positions of high density hotspots are marked by lower cases.

and calculated its frequency gradients. The decadic logarithm of the absolute value of the frequency gradients was calculated and plotted as a KDM by means of the statistical software PAST[d]. In detail this procedure is described in Kaufmann (2018).

3 Results

The observation was started at the beginning of 2018 shortly after the Quadrantids maximum. It was extended to mid-February. This time span was free of major meteor showers which allowed for an unbiased observation of the sporadic meteors. Table 1 outlines the result. The low number of head echoes is caused by the low radar cross section (RCS) of the plasma sheet, surrounding the travelling meteoroid. E.g. Close et al. (2002) found a maximum RCS of 0.14 m^2 at 160 MHz for the Leonids. So only head echoes from meteoroids of higher masses are captured.

A bar plot of the totalled hourly head echo counts of 40 days of observation is shown in Figure 1. Three peaks can be detected between $23^h - 02^h$, $04^h - 07^h$ and $10^h - 13^h$ UTC, respectively. To uncover continuous sources of sporadic meteors all frequency gradients of head echoes of the 40 day observation period were combined in one KDM, see Figure 1. For an insight in the sporadic meteor dynamics 4 consecutive KDM were created each comprising 10 days of observation, see Figure 2A–D. Each KDM displays the distribution of the measured frequency gradients in the time span $18^h - 17^h59^m$ UTC (local time CET = UTC + 1). Hot spots in a KDM mark a high number of similar frequency gradients.

At least to get an idea of the daily dynamics of sporadic meteors a ternary plot was created. For this purpose three timeframes were adopted and centred around the noticed three peaks of the hourly head echo counts (Figure 1). Each timeframe comprised three hours of observation: $23^h - 02^h$, $04^h - 07^h$ and $10^h - 13^h$ UTC. All observed head echoes being within these three timeframes were counted per day and depicted as daily proportion, see Figure 3. The number of head echoes within a timeframe is rather small (2–30). So random fluctuation within each timeframe will have a noticeable impact on their numeric proportions and must be taken in account.

4 Discussion

The bar plot of the hourly count rates of the head echoes (see Figure 1) exhibits three peaks. They occur at daytimes that coincide with the highest radiant positions in the sky of the AH, AP and H source, respectively (Lunsford, 2009). The proportion of these three peaks agrees with the measured activities of the AH, AP and H source by Campbell-Brown and Jones (2006). It can be assumed that these peaks are mainly the manifestation of the activity of the AH, AP and H source with minor contribution of the northern toroidal source as well as sporadic meteors that do not belong to one of these sources. Referring to the IMO 2018 working list (Rendtel, 2017) the GUM, DCS and DXC may be considered also.

The rising and falling of radiant positions due to Earth's rotation do not depict as tracks in the KDMs (Figure 1 and 2). This is due to the restricted sensitivity of the receiving system: only at a high altitude of the radiant the number of detectable head echoes is high enough to constitute noticeable densities becoming visible as hot spot in the KDM. Figure 1 and 2 are composed from several days of observation. So higher densities can result from persistent radiants of lower activity or short term radiants of higher activity.

The different hot spots emerge from clusters of common frequency slopes of the head echoes and indicate different radiant positions and/or geocentric velocities. In Figure 1 the hot spots exhibiting higher density are marked with lowercases a–n. They can be clustered into three groups by daytime which can be assigned to the AH (a–c), the AP (d–i) and to the H (j–n) peak of the head echo count rates. So for the period 2018 January 05 – February 14 at least 14 different major radiants could be distinguished basically within the AH, AP and H source by this technique. However there are more hot spots albeit of lesser density spread over the KDM. As

[d] http://folk.uio.no/ohammer/past/

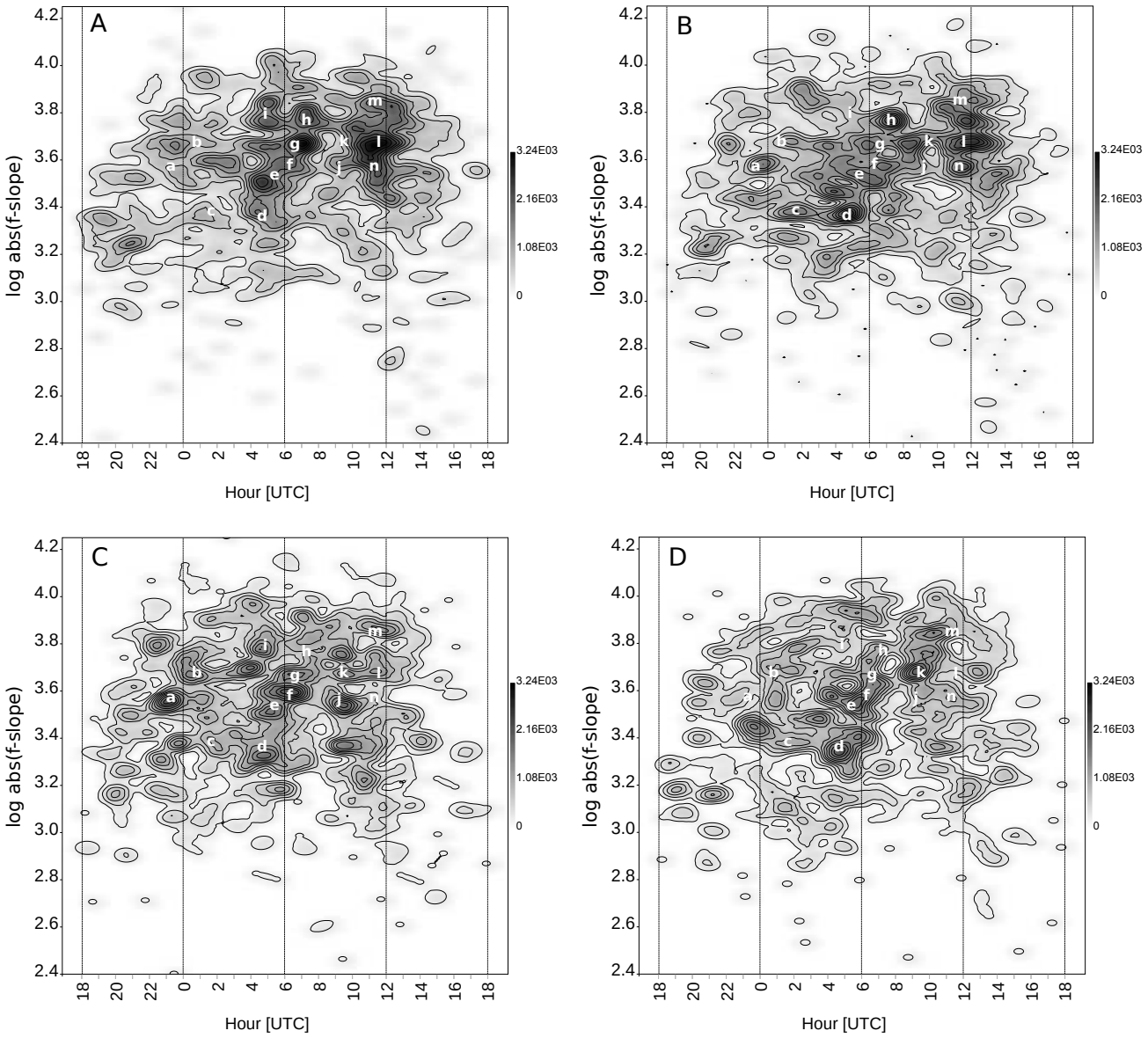

Figure 2 – Kernel density maps of the frequency slopes of head echoes each from 10×24 h of continuous observation: A) Jan 5 – Jan 15, B) Jan 15 – Jan 25, C) Jan 25 – Feb 04 and D) Feb 04 – Feb 14). Daily time span is $18^{\mathrm{h}} - 17^{\mathrm{h}}59^{\mathrm{m}}$ UTC. The positions marked by lower cases are copied from Figure 1.

weak showers they may be also part of the AH, AP and H source if occurring at the peak times of the head echo count rates.

Figures 2A to 2D give information about the persistence of the radiants of Figure 1. A comparison of the appearance of the marked radiants within the four intervals of the observation period (OBP) yields different trends, e.g.:

- a, b and c are most active in the middle of the OBP (2B, 2C),
- h is most active in the beginning of the OBP (2A, 2B),
- k is most active at the end of the OBP (2C, 2D),
- d is present over the complete OBP with a fluctuating activity,
- l is present over the complete OBP with a declining activity.

The major radiants of the AH, AP and H source obviously appear only for a limited period of time. So the AH, AP and H sources are composed of radiants not only differing in spatial position but also in time of activity.

Due to decreased averaging time in Figure 2 more weak short term radiants emerge. They are present only in one of the individual KDMs and are spread over the whole daytime and frequency gradient span. All in all the "continuous sporadic background" obviously is a result of a complex and highly irregular interplay of sporadic meteors in space and time. Belkovich (1995) stated that the radiant distribution is rather similar for the same time intervals in different years.

At least for an investigation of the daily dynamics of sporadic meteors the proportions of three specific daily count rates of head echoes are compiled in a ternary plot, see Figure 3. The specified portions of counts can be assigned mainly to the AH ($23^{\mathrm{h}}-02^{\mathrm{h}}$), AP ($04^{\mathrm{h}}-07^{\mathrm{h}}$)

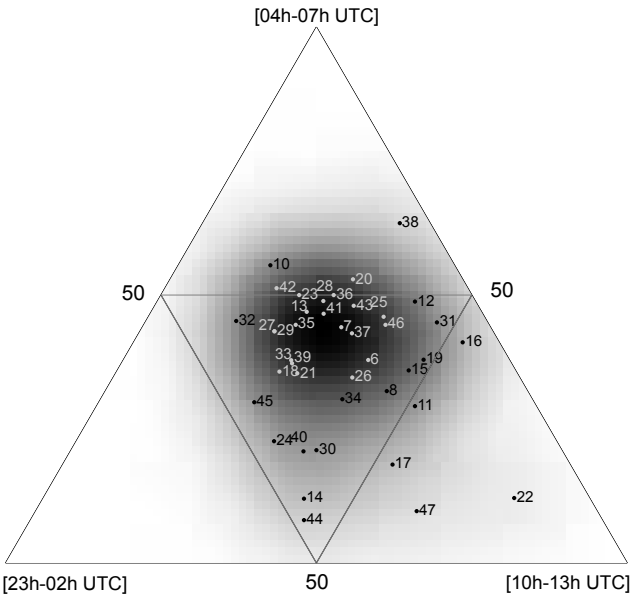

Figure 3 – Ternary plot of the daily proportions of the number of head echoes counted within each of the indicated timeframes (see also text). The dots were indexed by their calendar day (6–47 = Jan 6 – Feb 16). The point density is calculated by means of a kernel density method by the statistical software PAST.

and H ($10^{\mathrm{h}} - 13^{\mathrm{h}}$) source. A great variety of different proportions is shown. Ignoring the outliers as a result of the small numbers of counts no proportion seem to be preferred. The proportions are spread onto an area of circle as indicated by a circular point density distribution. The position of the centroid of the density distribution is determined by the mean proportion of the AH, AP and H activity. Furthermore the shape of the density distribution suggests a multivariate normal distribution of the combinations of activities of the AH, AP and H source. Hence consecutive calendar days do not show a trend in their proportions, the series of proportions is highly irregular.

This situation is the crux of numerical observations by radio forward scatter with a basic system: there is no procedure to precisely distinguish between the contribution of sporadic meteors and the shower under investigation. A widely used technique is to calculate a mean diurnal sporadic activity per hour from pre-recorded data that can be subtracted from the observed total number of counts per hour. The irregularity of the sporadic background nevertheless will imprint on the result. So smaller variations in the resulting counts per hour must not be interpreted unverified as changes in meteor flux or meteor mass distribution of the observed shower.

5 Conclusion

The technique of using frequency gradients of forward scattered head echoes to gain additional positional information demonstrated to be useful to:

- observe the concentration of sporadic meteors in the AH, AP and H source,
- differentiate major radiants in the AH, AP and H source (within the observing period 14 major radiants could be distinguished), and
- visualise the dynamics of the radiants within AH, AP and H sources as well as the dynamic occurrence of random weak and micro showers beyond these sources resulting in a continuous sporadic background.

The numerical analysis of the ratio of the activity of the AH, AP and H source on a daily base showed its high variability and unpredictability. Therefore using pre-recorded sporadic meteor counts for correction of subsequent shower records may be handled with care.

References

Belkovich O. I., Filimonova T. K., and Sidorov V. V. (1995). "Structure of sporadic meteor radiant distributions from radar observations". *Earth, Moon, and Planets*, **68**, 199–205.

Campell-Brown M. D. and Jones J. (2006). "Annual variation of sporadic radar meteor rates". *Mon. Not. R. Astron. Soc.*, **367:2**, 709–716.

Campell-Brown M. D. and Wiegert P. (2009). "Seasonal variations in the north toroidal sporadic meteor source". *Meteoritics and Planetary Science*, **44:12**, 1837–1848.

Close S., Oppenheim M., Hunt S., and Dryud L. (2002). "Scattering characteristics of high-resolution meteor head echoes detected at multiple frequencies". *J. Geophs. Res.*, **107:A10**. SIA 9 (1-12).

Hawkins G. S. (1956). "A radio echo survey of sporadic meteor radiants". *Mon. Not. R. Astron. Soc.*, **116**, 92–104.

Jones J. and Brown P. (1993). "Sporadic meteor radiant distribution: orbital survey results". *Mon. Not. R. Astron. Soc.*, **265**, 524–532.

Kaufmann W. (2017). "New radio meteor detecting and logging software". *WGN, Journal of the IMO*, **45:4**, 67–72.

Kaufmann W. (2018). "Visualizing meteor streams by radio forward scattering on the basis of meteor head echoes". *WGN, Journal of the IMO*, **46:1**, 39–44.

Lunsford R. (2009). *Meteors and How to Observe Them.* Springer, New York.

Rendtel J. (2017). "2018 Meteor Shower Calendar". International Meteor Organization, Potsdam. IMO_INFO (2-17).

Younger P. T., Astin I., Sandford D. J., and Mitchell N. J. (2009). "The sporadic radiant and distribution of meteors in the atmosphere as observed by VHF radar at Arctic, Antarctic and equatorial latitudes". *Ann. Geophys.*, **27**, 2831–2841.

Handling Editor: Jean-Louis Rault

Preliminary results

Results of the IMO Video Meteor Network — January 2018

Sirko Molau[1], Stefano Crivello, Rui Goncalves, Carlos Saraiva, Enrico Stomeo, Jörg Strunk, and Javor Kac

During 2018 January, cameras of the IMO Video Meteor Network recorded over 20 000 meteors in more than 8 000 hours of observing time. The Quadrantids were poorly covered by the Network cameras as the shower's short maximum occurred outside the observing window for most of the cameras. The descending branch of the flux density profile is shown and compared to profiles of years 2015 to 2017. The κ Cancrids did not appear in 2018. The flux density profile is presented for the γ Ursae Minorids, with the flux density below 1 meteoroid per 1 000 km^2 per hour between January 18 and 22.

Received 2018 December 23

1 Introduction

An otherwise spectacular year 2018 started with a meager January. Despite adding two new observers, Thomas Bianchi of Italy and Henrietta Nagy of Hungary, to our video network, our output was still well below that of previous years. Thomas operates the Mintron camera Omsl1 with a 4 mm Tamron lens in Mt. San Lorenzo. In the previous few months, Henrietta had taken over the support for a number of meteor cameras in Hungary. Here she is listed with the new camera Hupis, a Mintron camera with 3.8 mm Computar lens installed in Piszkéstető.

Overall 41 observers, with 79 meteor cameras, contributed to the IMO Network in January 2018. The first half of the month saw longer observing gaps at all observing sites due to poor weather, in the second half the observers in southern Europe, at least, could observe unhampered. Thus, only about ever third camera managed to observe during twenty or more observing nights in January. The effective observing time adds up to 8 000 hours (Table 1 and Figure 1), whereas in the previous three years we collected between 9 000 and 12 000 observing hours. With over 20 000 meteors, the meteor yield was also up to 40% smaller than in the preceding years.

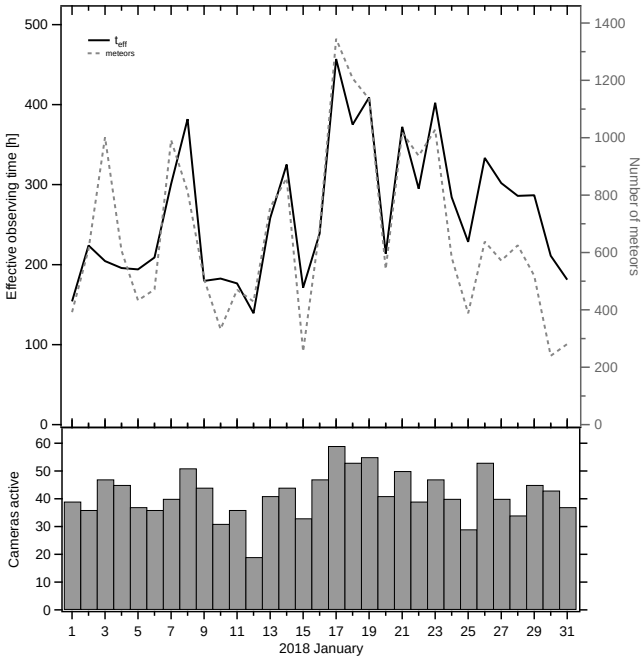

Figure 1 – Monthly summary for the effective observing time (solid black line), number of meteors (dashed gray line) and number of cameras active (bars) in 2018 January.

2 Quadrantids

Full moon right before the peak in combination with poor weather did not promise fine observing conditions for the first major shower of the year, the Quadrantids. During the night of 2018 January 3/4, we could record just about a thousand meteors. Figure 2 shows the activity profile of the Quadrantids. Due to their short peak, the profile is not really meaningful. It only tells us that during the aforementioned night we recorded more Quadrantids than during the nights before and after. Whether we really hit the peak (which is quite unlikely given the low flux density of 10 meteoroids per 1 000 km^2 per hour) can only be determined by comparing the data with the preceding years.

Figure 3 presents the flux density profile for the years 2015 to 2018. It shows that we indeed missed the peak in 2018. That far away from the maximum the rate was still considerable, but we should not forget that we do have a tendency to measure the flux density as being higher at full moon (Molau, 2016).

The population index in 2018 was derived from about 400 Quadrantids to be $r = 1.7$, compared with $r = 2.3$ for 200 sporadic meteors in the same time interval. That sounds plausible and matches with the values we obtained for 2013, 2014 and 2017. However, in other years, the population index has differed substantially, as can be seen in Figure 4. Particularly conspicuous are 2012 and 2016, when the Quadrantid peak occurred right before new moon and we measured population indices of $r = 2.5$. Furthermore, the sporadic population index was particularly small in 2012 and 2015.

If we compute a higher resolution population index profile from all years (Figure 5), this paradox is at least

[1]Abenstalstr. 13b, 84072 Seysdorf, Germany.
Email: sirko@molau.de

IMO bibcode WGN-466-molau-vidjan
NASA-ADS bibcode 2018JIMO...46..205M

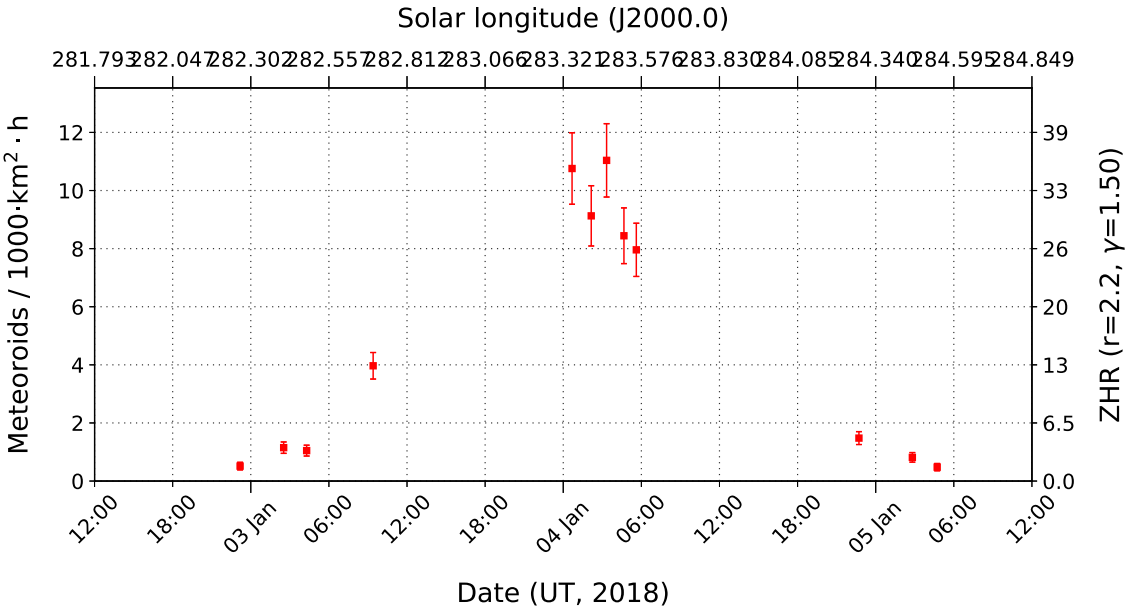

Figure 2 – Flux density profile of the Quadrantids in January 2018, derived from video data of the IMO Network.

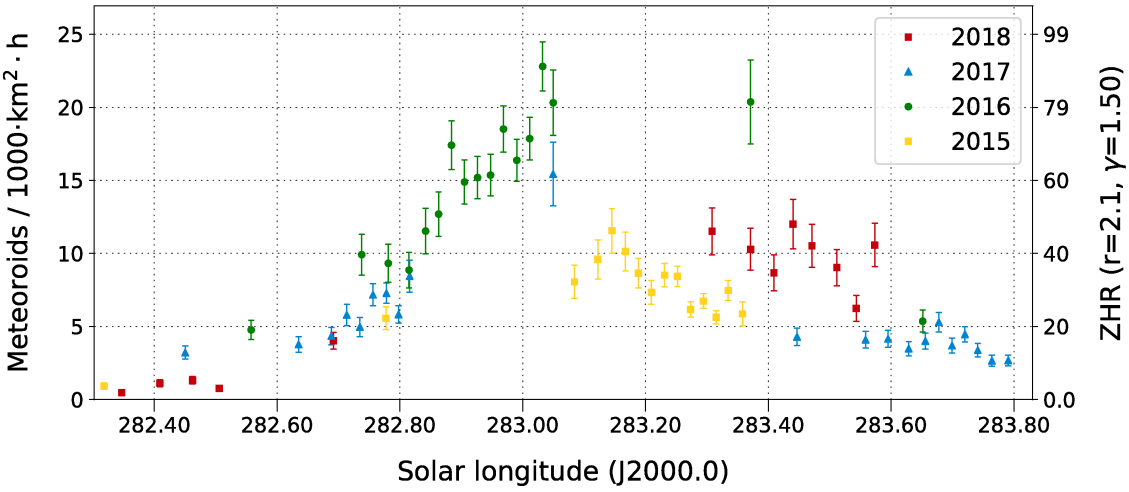

Figure 3 – Comparison of the flux density profile of the Quadrantids in 2014–2018, derived from video data of the IMO Network.

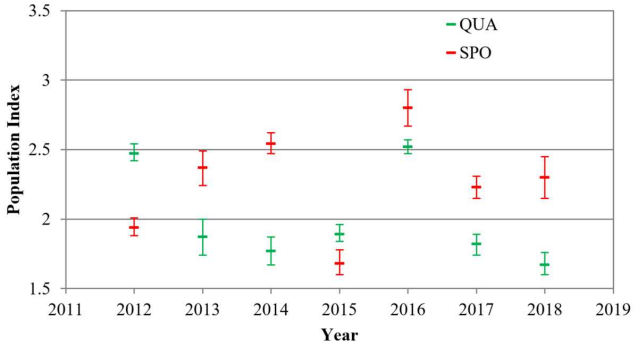

Figure 4 – Population index of the Quadrantids (lighter/green) and sporadic meteors (darker/red) in 2012–2018.

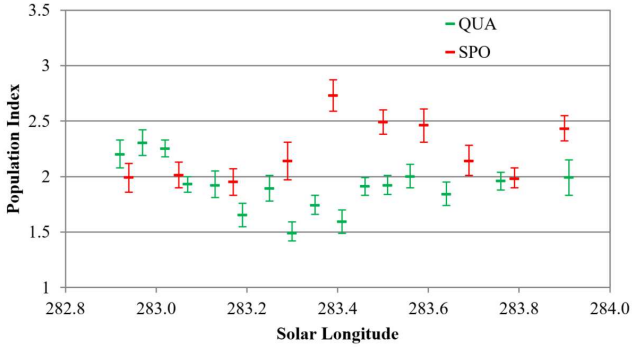

Figure 5 – Higher resolution average population index profile of the Quadrantids (lighter/green) and sporadic meteors (darker/red) in 2012–2018.

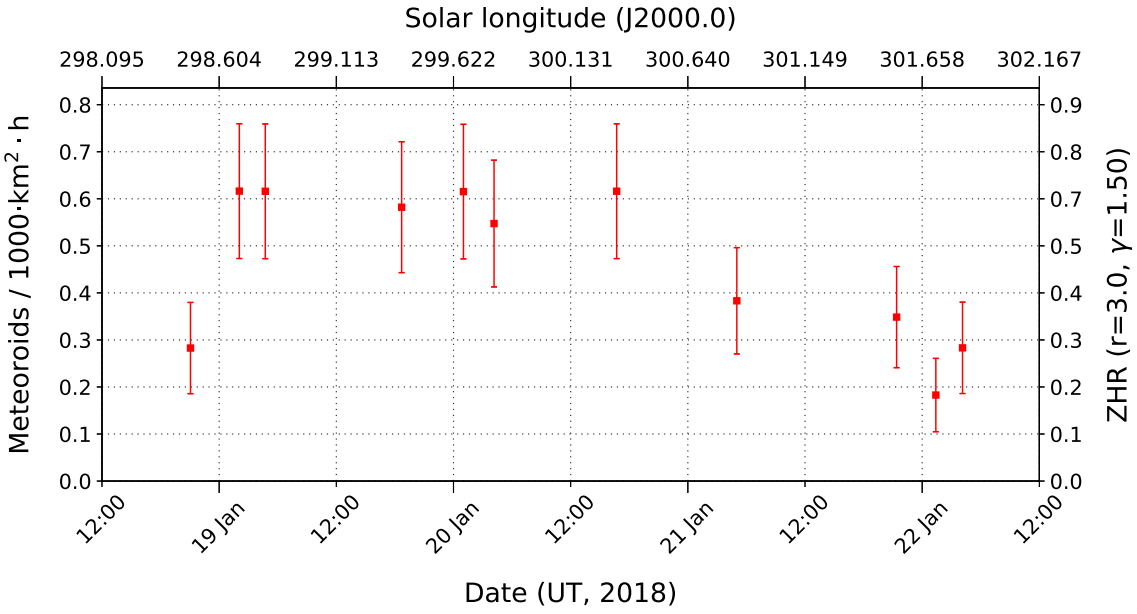

Figure 6 – Flux density profile of the γ Ursae Minorids in 2018 January, derived from video data of the IMO Network.

partially resolved. With $r = 2.3$ to $r = 2.0$, the population index at the start and end of the activity period is higher than at about 283°.3 solar longitude when the value decreases to $r = 1.6$. Since each year we observe only a fraction of the full activity profile in central Europe, we sometimes catch regions with a higher and in other years regions with a smaller population index. For this reason, the r-values are nearly identical every four years. The remaining variations can be attributed to different observing conditions (weather, lunar phase).

3 κ Cancrids

On 2015 January 9/10, we observed an extremely short outburst of the κ Cancrids with a FWHM of just 40 minutes (Molau et al., 2016). In more recent years, the shower has not been seen, although the peak time has been outside the European observing window. In 2018, we reached the corresponding solar longitude of 289°.315 on January 9 at $21^{\mathrm{h}}10^{\mathrm{m}}$ UT. That was still quite early in the night, but from most observing sites the radiant was already above 20° altitude, so that we should have seen an outburst of similar strength. A re-calculation of the shower assignment of all meteors yielded hardly any matches, though, and thus we can quite safely exclude another outburst in 2018.

4 γ Ursae Minorids

Finally, we checked if the minor shower of the γ Ursae Minorids was observed in 2018. The activity profile (Figure 6) shows slightly enhanced rates between January 18 and 20, but the flux density remained below one meteoroid per 1 000 km^2 per hour. The population index was clearly smaller than the sporadic r-value, but more detailed values could not be derived due to the small data set (150 shower meteors).

References

Molau S. (2016). "Flux density, population index, perception coefficient, and the Moon". In Roggemans A. and Roggemans P., editors, *International Meteor Conference Egmond, the Netherlands, 2-5 June 2016*. pages 185–191.

Molau S., Crivello S., Goncalves R., Saraiva C., Stomeo E., and Kac J. (2016). "Results of the IMO Video Meteor Network - February 2016". *WGN, Journal of the International Meteor Organization*, **44:4**, 116–119.

Handling Editor: Javor Kac

Code	Name	Location	Camera	FOV [°²]	Stellar LM [mag]	Eff.CA [km²]	Nights	Time [h]	Meteors
ARLRA	Arlt	Ludwigsfelde/DE	Ludwig2 (0.8/8)	1475	6.2	3779	19	78.4	285
BERER	Berkó	Ludányhalászi/HU	Hulud1 (0.8/3.8)	5542	4.8	3847	2	16.0	132
BIATO	Bianchi	Mt. San Lorenzo/IT	Omsl1 (1.2/4)	6435	4.0	1705	13	22.9	165
BOMMA	Bombardini	Faenza/IT	Mario (1.2/4.0)	5794	3.3	739	22	125.5	446
BREMA	Breukers	Hengelo/NL	Mbb3 (0.75/6)	2399	4.2	699	12	61.6	108
BRIBE	Klemt	Herne/DE	Hermine (0.8/6)	2374	4.2	678	19	65.7	132
		Bergisch Gladbach/DE	Klemoi (0.8/6)	2286	4.6	1080	15	47.1	81
CARMA	Carli	Monte Baldo/IT	Bmh2 (1.5/4.5)*	4243	3.0	371	23	240.6	1048
CASFL	Castellani	Monte Baldo/IT	Bmh1 (0.8/6)	2350	5.0	1611	21	220.8	431
CINFR	Cineglosso	Faenza/IT	Jenni (1.2/4)	5886	3.9	1222	19	30.9	213
CRIST	Crivello	Valbrevenna/IT	Arci (0.8/3.8)	5566	4.6	2575	21	173.5	512
			Bilbo (0.8/3.8)	5458	4.2	1772	21	177.9	641
			C3P8 (0.8/3.8)	5455	4.2	1586	17	156.4	384
			Stg38 (0.8/3.8)	5614	4.4	2007	21	167.9	871
ELTMA	Eltri	Venezia/IT	Met38 (0.8/3.8)	5631	4.3	2151	14	104.2	331
FORKE	Förster	Carlsfeld/DE	Akm3 (0.75/6)	2375	5.1	2154	6	11.1	42
GONRU	Goncalves	Foz do Arelho/PT	Farelho1 (0.75/4.5)	2286	3.0	208	17	126.6	76
		Tomar/PT	Templar1 (0.8/6)	2179	5.3	1842	23	198.4	538
			Templar2 (0.8/6)	2080	5.0	1508	24	208.3	457
			Templar3 (0.8/8)	1438	4.3	571	23	209.7	217
			Templar4 (0.8/3.8)	4475	3.0	442	23	199.9	415
			Templar5 (0.75/6)	2312	5.0	2259	25	204.2	427
GOVMI	Govedič	Središče ob Dravi/SI	Orion2 (0.8/8)	1447	5.5	1841	18	148.6	281
			Orion4 (0.95/5)	2662	4.3	1043	2	17.7	54
HERCA	Hergenrother	Tucson/US	Salsa3 (0.8/3.8)	2336	4.1	544	28	248.5	472
HINWO	Hinz	Schwarzenberg/DE	Hinwo1 (0.75/6)	2291	5.1	1819	13	55.4	97
IGAAN	Igaz	Budapest/HU	Hupol (1.2/4)	3790	3.3	475	12	74.8	47
JONKA	Jonas	Budapest/HU	Husor (0.95/4)	2286	3.9	445	17	93.0	124
			Husor2 (0.95/3.5)	2465	3.9	715	2	12.5	18
KACJA	Kac	Kamnik/SI	Cvetka (0.8/3.8)*	4914	4.3	1842	11	74.0	209
			Rezika (0.8/6)	2270	4.4	840	11	79.9	434
			Stefka (0.8/3.8)	5471	2.8	379	11	70.1	180
		Kostanjevec/SI	Metka (0.8/12)*	715	6.4	640	10	90.7	158
KOSDE	Koschny	Izana Obs./ES	Icc7 (0.85/25)*	714	5.9	1464	25	175.7	601
			Lic1 (2.8/50)*	2255	6.2	5670	25	221.2	834
		La Palma/ES	Icc9 (0.85/25)*	683	6.7	2951	2	22.8	201
			Lic2 (3.2/50)*	2199	6.5	7512	3	33.3	252
LOJTO	Łojek	Grabniak/PL	Pav57 (1.0/5)	1631	3.5	269	5	33.1	71
MACMA	Maciejewski	Chełm/PL	Pav35 (0.8/3.8)	5495	4.0	1584	13	42.3	97
			Pav36 (0.8/3.8)*	5668	4.0	1573	13	79.2	197
			Pav43 (0.75/4.5)*	3132	3.1	319	11	57.7	59
			Pav60 (0.75/4.5)	2250	3.1	281	14	84.0	194

Table 1 – Observers contributing to 2018 January data of the IMO Video Meteor Network. Eff.CA designates the effective collection area; the overall number of nights is the number of nights with at least one camera operating, the overall observing time and number of meteors are sums over all cameras.

Table 1 – Observers contributing to 2018 January data of the IMO Video Meteor Network – continued from previous page.

Code	Name	Location	Camera	FOV [°²]	Stellar LM [mag]	Eff.CA [km²]	Nights	Time [h]	Meteors
MARRU	Marques	Lisbon/PT	Cab1 (0.75/6)	2362	4.8	1517	26	190.9	469
			Ran1 (1.4/4.5)	4405	4.0	1241	26	198.9	539
MASMI	Maslov	Novosibirsk/RU	Nowatec (0.8/3.8)	5574	3.6	773	17	113.3	553
MOLSI	Molau	Seysdorf/DE	Avis2 (1.4/50)*	1230	6.9	6152	11	29.5	138
			Escimo2 (0.85/25)	155	8.1	3415	10	34.9	32
			Mincam1 (0.8/8)	1477	4.9	1084	12	25.3	100
		Ketzür/DE	Remo1 (0.8/8)	1467	6.5	5491	19	75.7	237
			Remo2 (0.8/8)	1478	6.4	4778	21	89.4	283
			Remo3 (0.8/8)	1420	5.6	1967	20	102.9	272
			Remo4 (0.8/8)	1478	6.5	5358	23	99.0	373
MORJO	Morvai	Fülöpszállás/HU	Huful (1.4/5)	2522	3.5	532	21	118.3	132
MOSFA	Moschini	Rovereto/IT	Rover (1.4/4.5)	3896	4.2	1292	21	149.7	196
NAGHE	Nagy	Piszkéstető/HU	Hupis (0.8/3.8)	5615	4.0	1524	16	28.0	109
OCHPA	Ochner	Albiano/IT	Albiano (1.2/4.5)	2944	3.5	358	14	20.9	50
OTTMI	Otte	Pearl City/US	Orie1 (1.4/5.7)	3837	3.8	460	22	160.2	281
PERZS	Perkó	Becsehely/HU	Hubec (0.8/3.8)*	5498	2.9	460	17	93.7	204
ROTEC	Rothenberg	Berlin/DE	Armefa (0.8/6)	2366	4.5	911	7	37.7	64
SARAN	Saraiva	Carnaxide/PT	Ro1 (0.75/6)	2362	3.7	381	18	134.3	228
			Ro2 (0.75/6)	2381	3.8	459	24	186.7	376
			Ro3 (0.8/12)	710	5.2	619	23	175.5	429
			Ro4 (1.0/8)	1582	4.2	549	24	165.6	145
			Sofia (0.8/12)	738	5.3	907	20	142.6	263
SCALE	Scarpa	Alberoni/IT	Leo (1.2/4.5)*	4152	4.5	2052	17	112.1	144
SCHHA	Schremmer	Niederkrüchten/DE	Doraemon (0.8/3.8)	4900	3.0	409	19	75.4	124
SLAST	Slavec	Ljubljana/SI	Kayak1 (1.8/28)	563	6.2	1294	8	50.9	153
			Kayak2 (0.8/12)	741	5.5	920	13	75.0	56
STOEN	Stomeo	Scorze/IT	Min38 (0.8/3.8)	5566	4.8	3270	20	142.1	659
			Noa38 (0.8/3.8)	5609	4.2	1911	5	24.8	102
			Sco38 (0.8/3.8)	5598	4.8	3306	21	161.9	610
STRJO	Strunk	Herford/DE	Mincam2 (0.8/6)	2354	5.4	2751	17	68.2	263
			Mincam3 (0.8/6)	2338	5.5	3590	16	66.1	115
			Mincam4 (0.8/6)	2306	5.0	1412	15	64.7	79
			Mincam5 (0.8/6)	2349	5.0	1896	14	60.8	131
			Mincam6 (0.8/6)	2395	5.1	2178	18	57.7	111
TEPIS	Tepliczky	Agostyán/HU	Huago (0.75/4.5)	2427	4.4	1036	15	82.6	208
			Humob (0.8/6)	2388	4.8	1607	14	97.4	147
WEGWA	Wegrzyk	Nieznaszyn/PL	Pav78 (0.8/6)	2286	4.0	778	17	72.3	159
YRJIL	Yrjölä	Kuusankoski/FI	Finexcam (0.8/6)	2337	5.5	3574	6	29.0	39
ZAKJU	Zakrajšek	Petkovec/SI	Tacka (0.8/12)	714	5.3	783	15	109.4	120
* active field of view smaller than video frame						Overall	31	8 172.2	20 672

History

A History of Meteor Reports in The Astronomer magazine: part 3 1990–1999

Tracie Heywood[1]

The magazine "*The Astronomer*" (TA) is a monthly magazine published in the UK whose aim is the rapid publication of observations made by amateur astronomers. It was first published in 1964. This is the third article in a series that provide an overview of the magazine's meteor content and covers the years 1990–1999.

Received 2018 September 30

1 Editorial and Sub-Editorial Changes

The 1990s are a period of anticipation and hope for meteor observers. Meteor storms from the Leonids in 1998 and/or 1999 are considered quite likely and there also seems to be a good chance of high, possibly storm level, rates from the Draconids in 1998. In addition, analysis of Perseid observations from around the world during the final years of the 1980s have indicated the presence of an additional earlier activity peak. There is speculation that this earlier peak might be a sign that the parent comet Swift-Tuttle is approaching perihelion (possibly in line with Brian Marsden's postulated "late" return date of 1992). This inevitably leads to further speculation that the proximity of Swift-Tuttle might, in turn, result in a significant increase in Perseid rates. In the 1991 November issue (Kidger, 1991b), for example, Mark Kidger looks at the viewing prospects for the comet that would result from various perihelion dates in the second half of 1992 and also speculates on possible Perseid rates for the 1992 and 1993 returns. Late September 1992 did bring the news that comet Swift-Tuttle had finally been recovered and would pass through perihelion on 1992 Dec 12.

When looking back at historical accounts of high meteor activity it is important, of course, to bear in mind that not everyone would have seen the outbursts. Some observers would have been clouded out. Some observers would have seen lower rates due to the outburst occurring with the radiant low in the sky. With outbursts being short-lived, outbursts would have been missed if they occurred during daylight or, in the case of the Leonids, before the radiant had risen. In addition, outbursts not predicted in advance would have been missed by many observers.

2 Perseids 1991–94

Let us look, for example, at the Perseid outbursts of the early 1990s, as "seen" by UK based observers.

1991: The "normal" Perseid peak of 1991 occurs just after New Moon. Much of the UK has clear skies and UK Perseid reports in the 1991 September issue (The Astronomer, 1991a) indicate that a fairly normal Perseid return has occurred. News has come through, however, via IAU Circular 5330, that observers in Japan have seen a sharp but intense burst of Perseid activity several hours ahead of the normal peak solar longitude.

1992: Moonlight circumstances for the peak of the 1992 Perseids are very unfavourable, with Full Moon occurring on August 13. The 1992 September issue (The Astronomer, 1992a) reveals that cloudy skies have hindered UK observations, but a report from Slovenia shows that another Perseid outburst has indeed occurred (during UK daylight hours) ahead of the 'normal' peak time.

1993: Perseid maximum in 1993 is eagerly anticipated. Moonlight circumstances are much more favourable than in 1992, the Moon having passed Last Quarter on August 10. Although the 'normal' Perseid peak is expected to occur at around $15^{\rm h}$ UT on August 12, the enhanced earlier peak is predicted to occur around 12 hours earlier. This will be close to or just after the end of the night for UK based observers. Reports published in the 1993 September issue (The Astronomer, 1993a) show that another outburst has indeed occurred with observers in Tenerife recording their highest Perseid rates between $03^{\rm h}00^{\rm m}$ and $03^{\rm h}30^{\rm m}$ UT. Peak rates have however fallen well short of storm levels. Once again, cloudy skies have hindered most UK based observers. Alastair McBeath is a noticeable exception, but the onset of morning twilight has ended his observations at $03^{\rm h}00^{\rm m}$ UT.

1994: Moonlight circumstances are good for the 1994 peak with the crescent Moon setting before midnight. The enhanced peak is, however, predicted to occur during UK morning daylight hours on August 12, favouring North America rather than Europe. The predicted outburst does occur, but with a lower peak level than in 1993. Observations reported in the 1994 September issue (The Astronomer, 1994a) show cloudy skies to have obstructed most UK observers during the night of August 11–12, leaving them having to make do with the clearer skies of the following night.

Thus, observers in the UK were unlucky. The 1992 enhancement occurred a little too early for UK observation while that of 1993 enhancement occurred a little too late. The 1991 and 1994 enhancements occurred during UK daylight hours. A study of Perseid rates in the years around the return of Swift-Tuttle, based solely on visual observations from the UK could have

[1]20 Hillside Drive, Leek, ST13 8JQ, UK.
Email: tracieheywood832@gmail.com

IMO bibcode WGN-466-heywood-ta3
NASA-ADS bibcode 2018JIMO...46..210H

mistakenly concluded that the parent comet's return had no effect on Perseid rates! This clearly highlights the benefits provided by worldwide monitoring of meteor activity in order to get the full picture.

3 ZHR calculations

The sharpness of the 1993 Perseid enhancement leads to a somewhat vigorous debate involving Mark Kidger, Neil Bone and John Bortle in the 1993 November (Bone, 1993), 1994 January (Bortle, 1994), 1994 February (Kidger, 1994) and 1994 March (Bone, 1994) issues, the key point being whether it is misleading to quote ZHRs extrapolated from intervals as short as 10 minutes.

4 Routine meteor watches

With so much attention being given to the possibility of enhanced Perseid and Leonid rates during the 1990s, other meteor showers could easily have been overlooked. Observations of other showers continue to be carried out, however.

In the 1990 January issue (Kidger, 1990), for example, Mark Kidger reports on observations of the 1989 Taurids from Tenerife. UK based reports, however, tend to focus on the most active showers. Many reports on Geminid meteor watches appear in the 1991 January (The Astronomer, 1991b) and 1994 January (The Astronomer, 1994b) issues, Quadrantid reports appear in the 1992 February issue (The Astronomer, 1992b) and Orionid reports appear in the 1993 November issue (The Astronomer, 1993b).

Meteor watches to study minor shower and sporadic activity are rare, however. This is presumably a consequence of the increasing problems of light pollution, noted at the end of the preceding part of this series of articles.

5 Unusual Meteors and Non-Meteors

Various items regarding unusual meteors appear, although there are less reports than in previous decades.

In the 1992 January issue (McNaught, 1991), Rob McNaught casts doubt on the existence of spiralling meteors, pointing out that none have been recorded on photographs from the UK Schmidt telescope while it has been operating normally.

In the 1993 July issue (McBeath, 1993), Alastair McBeath mentions the possibility (raised elsewhere a decade earlier) that meteor sound waves might be responsible for the moving ripples crossing solar haloes in high altitude aircraft contrails, these having been reported on a number of occasions. He suggests that the likely high meteor rates during the 1993 Perseid maximum might provide an opportunity for further sightings. In a follow up note in the 1994 March issue (McBeath, 1994), he reports that none of these effects were seen during the 1993 Perseids, but other similar events in earlier years have now come to light.

The 1993 December issue (Hurst & Hoeg, 1993) describes bright stationary long duration disk-like objects seen from North Sea oil rigs during the nights of 1993 October 20 and 1993 November 25. Since the first event occurred close to the peak of the Orionid meteor shower, a request had made to meteor observers in case any had seen the same or similar events. No such reports had come to light. An explanation for these events appears in the 1995 June issue (Hoeg, 1995). It had been deduced that the witnesses were seeing reflections, by crystals in high altitude cirrus cloud, of the gas flames from the oil platforms.

The 1994 May issue (Hurst, 1994a) contains reports of a fast-moving nebulous object seen crossing European skies during the evening of 1994 May 3. The object is reported to have started as a point source of around mag -4, which then became increasingly large and fuzzy, with later reports describing it reaching a diameter of around 2 degrees. An explanation for this event appears in the 1994 June issue (Hurst, 1994b), along with a number of images that had been captured. It is revealed to have been a vapour discharge from the Centaur upper stage of a US military Titan-IV rocket.

In the 1998 April issue (James, 1998), Nick James provides a short note about the Iridium satellites that are being launched, highlighting the very bright flares that they can produce. The front cover (Westlund, 1998) shows two of Margareta Westlund's images of an Iridium flare.

6 Imaging

Although CCD imaging almost completely replaces photographic film for other types of astronomical imaging during the 1990s, film continues to be the dominant method for meteor imaging, with most images featuring a backdrop of star trails. Images published include Daniel Fischer's photograph of two Perseids in the 1993 September issue (Fischer, 1993), Steve Evan's photograph of a Geminid in the 1994 January issue (Evans, 1994) and Gerhard Klaus' photograph of a Leonid fireball in the 1999 January issue (Klaus, 1999).

7 Video Observing

In the 1994 January issue (Evans & Elliott, 1994), Steve Evans and Andrew Elliott report on their results from simultaneous visual and video observations during the 1993 Geminids. This was part of a study into correlations between visual and video rates. It is noted that correlation between visual and video limiting magnitudes has still to be determined.

8 Triangulation

In the 1994 April issue (Howarth, 1994), Crayford House Astronomical Society report on their results from meteor triangulation during the 1993 Perseids. Although the UK has missed the peak in activity, they have captured images of one meteor from both locations and determined its atmospheric trajectory. Another attempt at triangulation is carried out during the 1996 Geminids, with the results being reported in the 1997 March issue (Crayford Manor House A. S., 1997).

Once again, one meteor, a mag −6 Geminid, has been imaged from two locations. The heights calculated are lower than expected, with the meteor starting at 80 km altitude and ending at 49 km altitude.

9 1995 Alpha Monocerotid outburst

The possibility of a short-lived outburst from this meteor shower received limited publicity in advance. The 1995 December issue (McBeath, 1995) does reveal, however, that Alastair McBeath has taken advantage of clearer post-midnight skies during the night of November 21–22 to detect a short-lived burst of activity, recording 24 Alpha Monocerotids between $01^{h}12^{m}$ and $01^{h}42^{m}$ UT.

10 Rising Leonid rates

When would Leonid rates start to pick up ahead of the possible 1998 or 1999 storms? As early as 1990, there were claims of higher than usual Leonid rates. Mark Kidger challenges these claims in the 1991 April issue (Kidger, 1991a), with further comments on ZHR calculations being added by Alastair McBeath.

Despite moonlit skies, significantly higher Leonid rates are reported from California in 1994, suggesting that rates are at last picking up ahead of the return of comet 55P/Tempel-Tuttle. UK reports in the 1995 December issue (The Astronomer, 1995) show that rates were again enhanced in 1995. There is uncertainty, however, regarding peak ZHR values. It is noted that the 1995 shower was rich in bright meteors and this raise questions as to whether appropriate correction values have been used when calculating ZHRs for 1994 and 1995.

The 1996 December issue (The Astronomer, 1996) reveals that most UK observers were clouded out for the Leonid peak, but notes that peak ZHRs of 60–70 were being suggested, based on reports from Canada and from elsewhere in Europe. In the 1997 January issue (The Astronomer, 1997a), John Bortle reports seeing fairly modest rates, *"not exceeding 35 per hour"*, adding *"the majority of meteors were zero magnitude or brighter, reminding me of the Leonid "fireball shower" of 1961. THERE WAS A MOST DECIDED LACK OF FAINT METEORS"*. He flags the implications that this will have for ZHR corrections.

Moonlight is a serious problem for observers of the 1997 Leonids. In the 1997 December issue (The Astronomer, 1997b), Josep M Trigo y Rodriguez, observing visually from Spain, reports having experienced a memorable three hours during the morning of November 17, estimating the ZHR to be near 100. Observations by the AFAM Radio Astronomy Group in Italy reveal peak radio meteor activity to have occurred at $10^{h}50^{m}$ UT.

11 1998 June Bootid outburst

Although the June Bootids had produced a number of outbursts in the early 20th century, the assumption was that the meteor stream was no longer encountering the Earth and so no significant activity was likely anymore. The outburst during the night of 1998 June 27–28 therefore takes observers by surprise and this may well explain the lack of agreement between witnesses as to the precise location of the radiant in northern Bootes. The 1998 July issue (The Astronomer, 1998a) includes reports of observations of the outburst by members of Unione Astrofili Italiani.

12 1998 Draconid outburst

The Draconids had produced an unexpected outburst in 1985 and, two orbits later, there is hope of another outburst in 1998. In 1998, the method for assessing the likelihood of future meteor storms is still primarily based on how close the Earth will pass to the parent comet's orbit. Closest passage to the orbit of the parent comet Giacobini-Zinner in 1998 is set to occur at approx. 21^{h} UT on October 8. It is assumed that any enhancement in rates will occur close to this time. If correct, this will be favourable for observers in the UK and western Europe, but observers further east will be less favoured.

The 1998 November issue (The Astronomer, 1998b) includes several reports of Draconid activity. Colin Henshaw in Saudi Arabia has recorded 17 Draconids between $15^{h}10^{m}$ and $17^{h}10^{m}$ UT (LM 5.1), while Margareta Westlund in Sweden has recorded 10 Draconids between $17^{h}35^{m}$ and $21^{h}00^{m}$ UT, adding *"Nice to see them, but I had expected more"*. Enrico Stomeo (Italy) and Alastair McBeath (UK), having had to wait later for skies to darken, have seen lower rates.

An outburst of activity has occurred, but the peak has been prior to any of these observations. IAU Circular 7027 reports that visual and video observers in Japan recorded an outburst at around October 8.56 UT, this being 7 hours ahead of the closest approach to the comet's orbit.

13 Surprises from the 1998 Leonids

Predictions, based on when the Earth would pass closest to the orbit of the parent comet Tempel-Tuttle, indicate that the best chance for a Leonid meteor storm in 1998 will be at around 19^{h} UT on November 17th. This is too early for visual observation from most of Europe. Eastern Asia seems better placed at this time and thus many observers head out to locations in this area. From Europe, the best night is expected to be November 17–18, catching the decline from any storm activity that has occurred. Nothing special is expected on November 16–17, although observations that night would still be useful for establishing the shape of the activity curve.

The night of November 16–17 starts cloudy in the UK. Conditions improve later in the night, although observing conditions for many remain far from optimal. Some observers make the mistake of going to bed in order to "save their efforts" for the following night. Those that venture outside are rewarded with a spectacular display containing a high percentage of bright meteors. TA E-Circular 1358, issued at 07:32 on November 19,

Tony Markham (Leek, England)

Date	Times(UT)	Durn	AvCld	LM	Leo	Tau-N	Tau-S	Spor
Nov 15/16	0337-0437	1h00m	-	5.5	6	1	1	4
	0437-0545	1 08	-	5.4	7	0	0	5
16/17	0325-0355	0 30	*	*	41	0	0	1
	0355-0425	0 30	*	*	47	0	0	1
	0425-0455	0 30	*	*	52	0	0	0
	0455-0525	0 30	5%	5.1	52	0	0	0
	0525-0555	0 30	7%	5.0-4.1	49	0	0	1
	0555-0620	0 25	10%	4.1-3.2	34	0	0	1
17/18	2211-2241	0 30	8%	5.2	0	2	0	0
	2241-2311	0 30	70%	5.0	1	0	0	0
	2311-2341	0 30	15%	5.0-4.2	0	0	0	1
	2341-0003	0 22	10%	4.3	1	0	1	0

- the asterisks indicate that the cirrus was so patchy and variable that it wasn't possible to quote a meaningful average LM or cloud value.
Highlights included 5 meteors in the first minute and 8 meteors in a minute at 0449UT. The mag -4 meteors were at 0345 (Col/Eri),0421 (no stars visible), 0443 (Tau) and 0459 (Sex to Hya) - the latter, low down in cirrus probably matches Neil Bone's mag -8 (see later). After the end of the watch a bright flash from overhead (UMa) occured at 0628UT - the fireball wasn't seen directly, but was probably around mag -6.

Magnitudes (Nov 16/17)

	NSV	-4	-3	-2	-1	0	1	2	3	4	Total	Trains
Leonids	5	4	6	13	36	40	84	61	24	2	275	140
Sporadics							1	3	0	0	4	0

- the NSV column identifies meteors seen in a part of the sky in which no stars were currently visible (due to thin cloud). Obviously some magnitudes and trains may have been affected by the thin cloud

Figure 1 – Tony Markham's report of the 1998 Leonids.

includes extracts from emails received from several observers, illustrating that the enhanced rates have been seen over prolonged period from many locations around the world:

Gabriel Oksa:
1998 November 16/17, 4:45 to 4:55 UT I saw around 20 Leonid bolides, each brighter than −1 mag, two of them like lightening in storm, around −10 mag. This was in the middle of town Trnava (Slovakia) with severe light pollution! Bolides were beautifully orange, very rapid, each had train. During my way to work in the bus I saw another five bolides in bright twilight, the last one at 5:25 UT near the Moon just over horizon, it was like full moon !!!

Jim Kremsreiter:
Leonid report from midwest USA. While flying between Detroit, Michigan and Madison, Wisconsin between 0530 and 0645 UT, Nov 16, 1998 I saw about 30 bright meteors. Quite a few to about Mag −4. The weather was solid overcast during that period so the only way to see anything was to fly. I was flying west, away from Leo, so I figured I missed most of the dimmer meteors.

Martin Brown:
Nov 16/17, 0700-0800 GMT+1 from Belgium I saw several bright meteors in mag −5 brightness range and the odd one with persistent trail. Light pollution in Brussels is a bit severe so only the brightest meteors were visible from my location. Arcturus was lost in dawn sky brightness from high cloud at around 0740, but meteors still visible.

whereas the enhancement was not seen from Australia later on November 17th:

Fraser Farrell (Australia):
During the observing period (Nov 17 16:30 to 18:40UT) I saw 39 Leonids. About the same rate as I saw in 1997, but most of this year's Leonids were bright (mags −3 to 1) with many leaving long, brief, trails.

Eastern Asia, somewhat ironically, is in the longitude range least well placed to see this broad early peak. For some travellers, the weather has also been unfavourable. They do, at least, see enhanced rates at the time of the nodal passage, but these are not only well short of storm level, but are also lower than the enhanced rates seen from Europe the previous night.

Nick James:
Reports from the Mason/Mobberley
India expedition indicate that rates were only around 40/hr at the predicted storm peak (Nov 17.8). No observing was possible on the previous night due to a Cyclone!

The November 16–17 event soon becomes known as the "Leonid Fireball Storm", but had it been a storm? Many observers having seen the event in poor sky conditions, assume that they have missed many fainter meteors and that adding these in will take the ZHR to storm levels. Some subsequent media reports do claim ZHR values as high as 2000, but analyses derived from observations with better limiting magnitudes reveal that these fainter Leonids had not been present in such numbers and therefore conclude that the ZHR has been well below storm level.

Had observers who had travelled to Eastern Asia been misled by unreliable predictions?

The Meteor Notes column in the December issue quotes from the IMO Circular of November 18. This had addressed both of the above issues and regarding the latter question stated:

"The peak is not wrong or shifted by 16 hours. The Leonid meteor shower consists of two components: A storm component of mostly faint meteors, and a back-

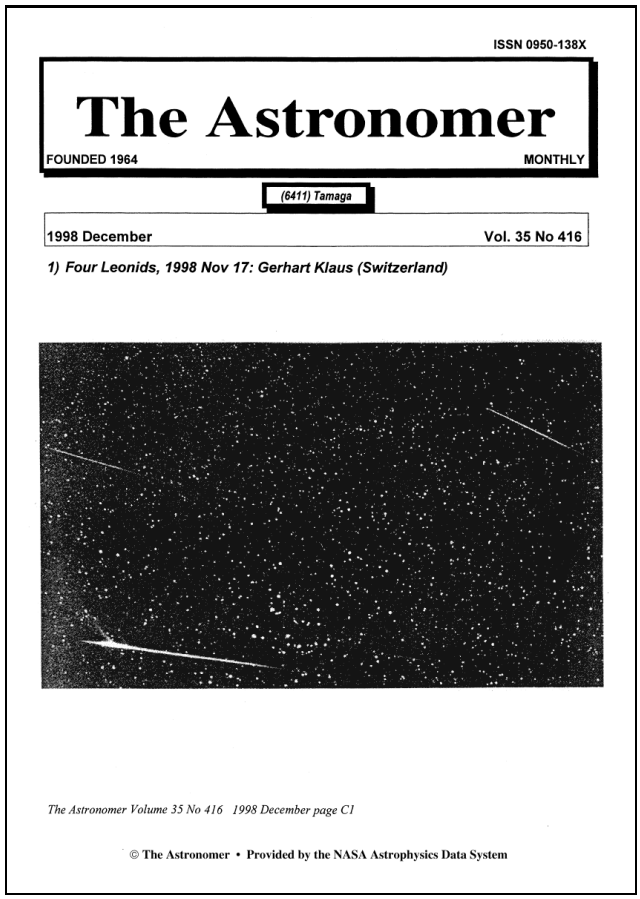

Figure 2 – December 1998 issue cover.

ground component rich in bright meteors. The high activity observed between Nov 17.0 and 17.5 UT was most likely a strong background component being several revolutions around the Sun old. It is very naturally off any prediction. THE PEAK DID OCCUR, BUT VERY INDISTINCTLY AT Nov 17.8 UT WITH RATES OF $\sim$ 150 *METEORS PER HOUR".*

Many more reports of the November 16–17 event appear in the Meteor Notes column in the 1998 December issue (The Astronomer, 1998c). The front cover (Klaus, 1998) shows an image captured during a 15-minute exposure by Gerhart Klaus that shows four Leonids. Martin Mobberley reports (Mobberley, 1998) on the experiences of a group observers who had travelled to India in a report titled *"Leonid 1998 Nightmare in Darjeeling".* Further Leonid reports appear in the 1999 January issue (The Astronomer, 1999a) and February issues (The Astronomer, 1999b), including detailed accounts from Daniel Fischer (Mongolia) (Fischer, 1999) and Stephen Lubbock (La Palma) (Lubbock, 1999).

14 A new era in Leonid Predictions

An article by Rob McNaught in the 1999 March issue (McNaught, 1999b) heralds a new era in meteor storm prediction. Rather than focussing on when and how close the Earth will pass to the orbit of the parent comet, this models the evolution of dust trails left behind by previous returns of the parent comet. Modelling the evolution of the dust trails backwards in time has been found to make predictions that tie in well with the timings of previously observed meteor storms and to also explain the absence of storms in other years.

The article makes predictions for future Leonid meteor storms. In particular, based on dust trail calculations by David Asher, it predicts a Leonid meteor storm that will peak at $02^{\rm h}08^{\rm m}$ UT on 1999 November 18. Although this is only around an hour different from predictions based on proximity to the comet's orbit, the method also predicts that additional, previously unforeseen, storms will occur in 2001 and 2002. Further information about the method is provided in the 1999 November issue (McNaught, 1999a).

15 The 1999 Leonid storm

Buoyed by the Asher & McNaught predictions, many meteor observers head out to Egypt, eastern Europe and western Asia and are rewarded with meteor storm activity. Highly significant is that the observations show the peak to have occurred within a few minutes of the time predicted by Asher & McNaught, a great success for the new prediction method.

The 1999 December issue (The Astronomer, 1999c) includes many reports of the Leonid storm. Mark Kidger reports on observations made from Tenerife, Andreas Kammerer reports observations made with a colleague from southern France, Melvyn Taylor reports his observations from Cyprus and results from Unione Astrofili Italiani group also appear. Martin Mobberley provides a detailed account (Mobberley, 1999) of an expedition to see the storm from Sinai.

In contrast, observers who remained in the UK have mostly been disappointed, enduring overcast skies. Only two UK reports, from Alastair McBeath in NE England and by Peter Guest in eastern Scotland, appear. Both see the storm period, but their view is badly affected by cloud.

16 In conclusion

The 1990s proved to be an exciting decade for meteor observers, dominated by the anticipation of outbursts of meteor activity. The decade had ended with the outstanding success of a new method for predicting meteor outbursts. Furthermore, this new method was predicting that Leonid meteor storms were also likely in 2001 and 2002. Meteor outbursts aside, however, visual meteor observing was continuing to struggle and technology limitations were limiting the take up of new imaging methods. This would change, however, over the next decade.

References

Bone N. M. (1993). "Perseids". *The Astronomer*, **30:355**, 166. [7:166].

Bone N. M. (1994). "Meteor Notes". *The Astronomer*, **30:359**, 259. [11:259].

Bortle J. (1994). "Meteor Notes". *The Astronomer*, **30:357**, 206. [9:206].

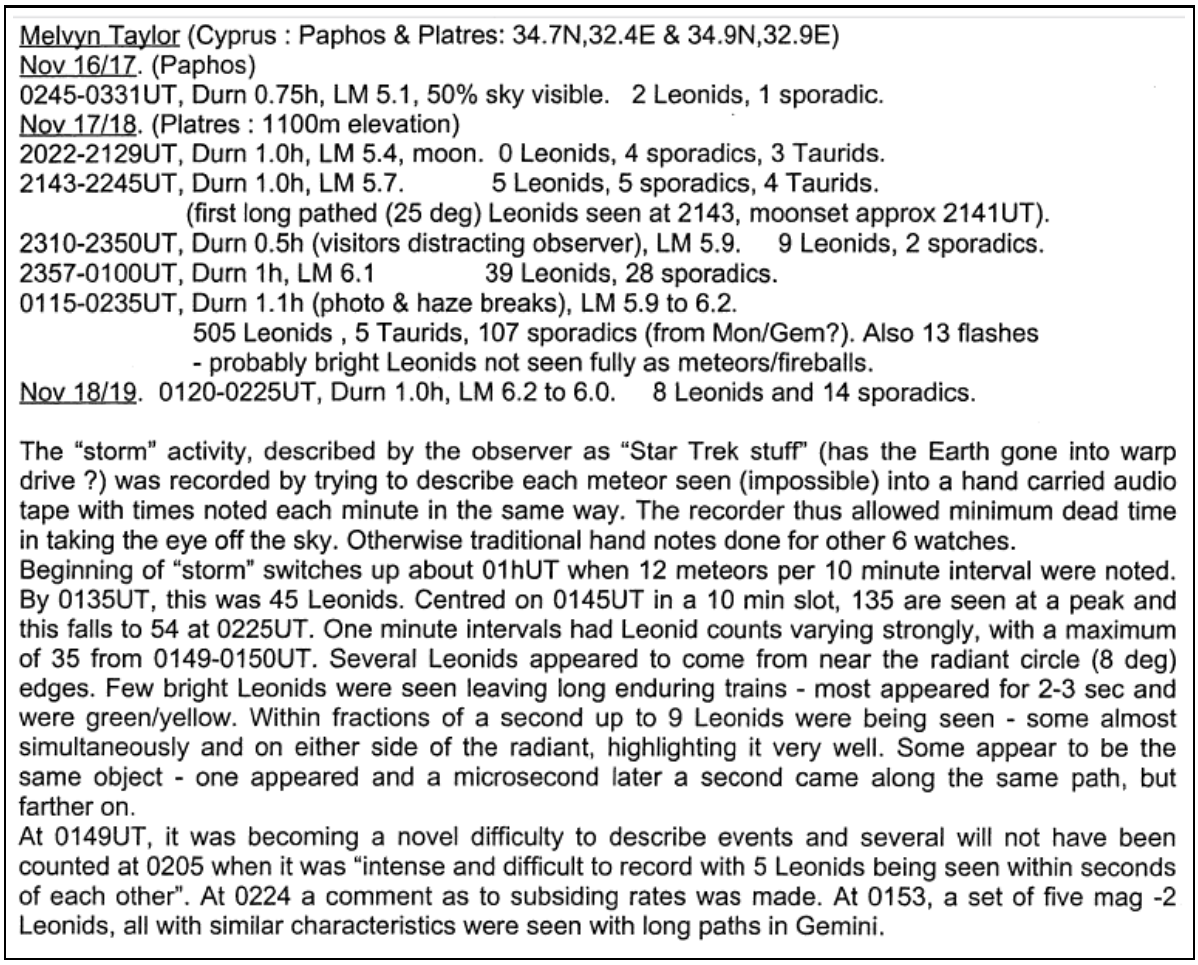
Melvyn Taylor (Cyprus : Paphos & Platres: 34.7N,32.4E & 34.9N,32.9E)
Nov 16/17. (Paphos)
0245-0331UT, Durn 0.75h, LM 5.1, 50% sky visible. 2 Leonids, 1 sporadic.
Nov 17/18. (Platres : 1100m elevation)
2022-2129UT, Durn 1.0h, LM 5.4, moon. 0 Leonids, 4 sporadics, 3 Taurids.
2143-2245UT, Durn 1.0h, LM 5.7. 5 Leonids, 5 sporadics, 4 Taurids.
(first long pathed (25 deg) Leonids seen at 2143, moonset approx 2141UT).
2310-2350UT, Durn 0.5h (visitors distracting observer), LM 5.9. 9 Leonids, 2 sporadics.
2357-0100UT, Durn 1h, LM 6.1 39 Leonids, 28 sporadics.
0115-0235UT, Durn 1.1h (photo & haze breaks), LM 5.9 to 6.2.
505 Leonids , 5 Taurids, 107 sporadics (from Mon/Gem?). Also 13 flashes
- probably bright Leonids not seen fully as meteors/fireballs.
Nov 18/19. 0120-0225UT, Durn 1.0h, LM 6.2 to 6.0. 8 Leonids and 14 sporadics.

The "storm" activity, described by the observer as "Star Trek stuff" (has the Earth gone into warp drive ?) was recorded by trying to describe each meteor seen (impossible) into a hand carried audio tape with times noted each minute in the same way. The recorder thus allowed minimum dead time in taking the eye off the sky. Otherwise traditional hand notes done for other 6 watches.
Beginning of "storm" switches up about 01hUT when 12 meteors per 10 minute interval were noted. By 0135UT, this was 45 Leonids. Centred on 0145UT in a 10 min slot, 135 are seen at a peak and this falls to 54 at 0225UT. One minute intervals had Leonid counts varying strongly, with a maximum of 35 from 0149-0150UT. Several Leonids appeared to come from near the radiant circle (8 deg) edges. Few bright Leonids were seen leaving long enduring trains - most appeared for 2-3 sec and were green/yellow. Within fractions of a second up to 9 Leonids were being seen - some almost simultaneously and on either side of the radiant, highlighting it very well. Some appear to be the same object - one appeared and a microsecond later a second came along the same path, but farther on.
At 0149UT, it was becoming a novel difficulty to describe events and several will not have been counted at 0205 when it was "intense and difficult to record with 5 Leonids being seen within seconds of each other". At 0224 a comment as to subsiding rates was made. At 0153, a set of five mag -2 Leonids, all with similar characteristics were seen with long paths in Gemini.

Figure 3 – Melvyn Taylor's report of the 1999 Leonids.

Crayford Manor House A. S. (1997). "Triangulation of a Geminid meteor". *The Astronomer*, **34:408**, 256. [1:256].

Evans S. (1994). "Geminid meteor, 1993 Dec 14". *The Astronomer*, **30:357**, C3. [Cover 12:Z1].

Evans S. and Elliott A. (1994). "Video observations, visual observations, conventional photography". *The Astronomer*, **30:357**, 206. [9:206].

Fischer D. (1993). "Perseid meteors". *The Astronomer*, **30:353**, C3. [Cover 12:Z1].

Fischer D. (1999). "The 1998 Leonids – The Mongolian view". *The Astronomer*, **35:417**, 223. [9:223].

Hoeg E. (1995). "Explanation of the Light Phenomenon over gas platforms, observed in 1993 Oct/Nov". *The Astronomer*, **32:374**, 33. [2:33].

Howarth, J. et al. (1994). "Triangulation of a Perseid meteor". *The Astronomer*, **30:360**, 281. [12:281].

Hurst G. M. (1994a). "Fast-moving nebulous object of 1994 May 3". *The Astronomer*, **31:361**, 17. [1:17].

Hurst G. M. (1994b). "Vapour cloud release from a US Military Titan-IV Centaur". *The Astronomer*, **31:362**, 37. [2:37].

Hurst G. M. and Hoeg E. (1993). "Disk-Like Objects of 1993 Oct 20 and Nov 25". *The Astronomer*, **30:356**, 188. [8:188].

James N. D. (1998). "Iridium flares". *The Astronomer*, **34:408**, 299. [12:299].

Kidger M. (1991a). "ZHR Calculation for the 1990 Leonids". *The Astronomer*, **27:324**, 263. [12:263].

Kidger M. R. (1990). "Agrupacion Astronomica de Tenerife". *The Astronomer*, **26:309**, 200. [10:200].

Kidger M. R. (1991b). "Comet Swift-Tuttle". *The Astronomer*, **28:331**, 164. [7:164].

Kidger M. R. (1994). "Meteor Notes". *The Astronomer*, **30:358**, 232. [10:232].

Klaus G. (1998). "Four Leonids, 1998 Nov 17". *The Astronomer*, **35:416**, C1. [Cover 8:1].

Klaus G. (1999). "Leonid, 1998 Nov 17". *The Astronomer*, **35:417**, C2. [Cover 9:2].

Lubbock S. (1999). "Leonid meteors 1998 – Roque de los Muchachos, La Palma – 2426m". *The Astronomer*, **35:418**, 254. [10:254].

McBeath A. (1993). "Visual meteor sound observations?". *The Astronomer*, **30:351**, 62. [3:62].

McBeath A. (1994). "Meteor Notes". *The Astronomer*, **30:359**, 260. [11:260].

McBeath A. (1995). "Meteor Notes". *The Astronomer*, **32:380**, 183. [8:183].

McNaught R. H. (1991). "Wobbly Ideas: Photographs of 'spiralling meteors'". *The Astronomer*, **27:321**, 190. [9:190].

McNaught R. H. (1999a). "Leonid dust trail prediction for 1999". *The Astronomer*, **36:427**, 171. [7:171].

McNaught R. H. (1999b). "On predicting the time of Leonid storms". *The Astronomer*, **35:419**, 279. [11:279].

Mobberley M. (1998). "Leonid 1998 nightmare in Darjeeling – My personal surreal experience". *The Astronomer*, **35:416**, 193. [8:193].

Mobberley M. (1999). "Leonid 99 success in Sinai - extracts from the diary of Martin Mobberley". *The Astronomer*, **36:428**, 194. [8:194].

The Astronomer (1991a). "Meteor notes". *The Astronomer*, **28:329**, 114. [5:114].

The Astronomer (1991b). "Meteor notes". *The Astronomer*, **27:321**, 199. [9:199].

The Astronomer (1992a). "Meteor notes". *The Astronomer*, **29:341**, 116. [5:116].

The Astronomer (1992b). "Meteor notes". *The Astronomer*, **28:334**, 236. [10:236].

The Astronomer (1993a). "Meteor notes". *The Astronomer*, **30:353**, 118. [5:118].

The Astronomer (1993b). "Meteor notes". *The Astronomer*, **30:355**, 165. [7:165].

The Astronomer (1994a). "Meteor notes". *The Astronomer*, **31:365**, 120. [5:120].

The Astronomer (1994b). "Meteor notes". *The Astronomer*, **30:357**, 206. [9:206].

The Astronomer (1995). "Meteor notes". *The Astronomer*, **32:380**, 181. [12:281].

The Astronomer (1996). "Meteor notes". *The Astronomer*, **33:392**, 181. [1:281].

The Astronomer (1997a). "Meteor notes". *The Astronomer*, **33:393**, 205. [1:205].

The Astronomer (1997b). "Meteor notes". *The Astronomer*, **34:404**, 198. [8:198].

The Astronomer (1998a). "Meteor notes". *The Astronomer*, **35:411**, 70. [3:70].

The Astronomer (1998b). "Meteor notes". *The Astronomer*, **35:415**, 164. [7:164].

The Astronomer (1998c). "Meteor notes". *The Astronomer*, **35:416**, 196. [8:196].

The Astronomer (1999a). "Meteor notes". *The Astronomer*, **35:417**, 223. [9:223].

The Astronomer (1999b). "Meteor notes". *The Astronomer*, **35:418**, 253. [10:253].

The Astronomer (1999c). "Meteor notes". *The Astronomer*, **36:428**, 197. [8:197].

Westlund M. (1998). "Iridium 12 flare, 1998 Feb 10". *The Astronomer*, **34:408**, C1. [Cover 12:1].

Back issues of most issues of the magazine have been uploaded to the NASA ADS system and can be downloaded via this link on the magazine's home page: `http://www.theastronomer.org/post/NASA%20ADS/`

Unfortunately, the page-ids stored in the NASA ADS system don't always directly match the page numbers from the printed magazine. To help mitigate this problem, those page-ids that differ from the printed values have been included (when available) in brackets at the end of each reference.

Handling Editor: Javor Kac

The International Meteor Organization

www.imo.net

Follow us on Facebook InternationalMeteorOrganization

Follow us on Twitter @IMOMeteors

Council

President: Cis Verbeeck,
Bogaertsheide 5, 2560 Kessel, Belgium.
e-mail: cis.verbeeck@scarlet.be

Vice-President: Juraj Tóth,
Fac. Math., Phys. & Inf., Comenius Univ.,
Mlynska dolina, 84248 Bratislava, Slovakia.
e-mail: toth@fmph.uniba.sk

Secretary-General: Robert Lunsford,
14884 Quail Valley Way, El Cajon,
CA 92021-2227, USA. tel. +1 619 755 7791
e-mail: lunro.imo.usa@cox.net

Treasurer: Marc Gyssens, Heerbaan 74,
B-2530 Boechout, Belgium.
e-mail: marc.gyssens@uhasselt.be
BIC: GEBABEBB
IBAN: BE30 0014 7327 5911
Bank transfer costs are always at your expense.

Other Council members:

Megan Argo, Jodrell Bank Centre for Astrophysics,
Alan Turing building, University of Manchester,
Oxford Road, Manchester, M13 9PL, UK.
e-mail: megan.argo@gmail.com

Javor Kac (see details under WGN)

Detlef Koschny, Zeestraat 46,
NL-2211 XH Noordwijkerhout, Netherlands.
e-mail: detlef.koschny@esa.int

Masahiro Koseki, 4-3-5 Annaka, Annaka-shi,
Gunma-ken 379-0116, Japan.
e-mail: geh04301@nifty.ne.jp

Sirko Molau, Abenstalstraße 13b, D-84072 Seysdorf,
Germany. e-mail: sirko@molau.de

Jean-Louis Rault, Société Astronomique de France,
16, rue de la Vallée, 91360 Epinay sur Orge,
France. e-mail: f6agr@orange.fr

Jürgen Rendtel, Eschenweg 16, D-14476 Marquardt,
Germany. e-mail: jrendtel@aip.de

Paul Roggemans, Pijnboomstraat 25, 2800 Mechelen,
Belgium, e-mail: paul.roggemans@gmail.com

Galina Ryabova, Res. Inst. of Appl. Math. & Mech.,
Tomsk State University, Lenin pr. 36, build. 27,
634050 Tomsk, Russian Federation.
e-mail: ryabova@niipmm.tsu.ru

Damir Šegon, J. Rakovca 3, 52100 Pula, Croatia.
e-mail: damir.segon@pu.t-com.hr

Commission Directors

Visual Commission: Rainer Arlt (rarlt@aip.de)
Generic e-mail address: visual@imo.net
Electronic visual report form:
http://www.imo.net/visual/report/electronic

Video Commission: Sirko Molau (video@imo.net)

Photographic Commission: Bill Ward
(William.Ward@glasgow.ac.uk)
Generic e-mail address: photo@imo.net

Radio Commission: Jean-Louis Rault (radio@imo.net)

Fireballs: Online fireball reports:
http://fireballs.imo.net

Outreach Officer

Jure Atanackov, e-mail: jureatanackov@gmail.com

Webmaster

Karl Antier, e-mail: webmaster@imo.net

WGN

Editor-in-chief: Javor Kac
Na Ajdov hrib 24, SI-2310 Slovenska Bistrica,
Slovenia. e-mail: wgn@imo.net;
include METEOR in the e-mail subject line

Editorial board: Ž. Andreić, M. Argo, D.J. Asher,
F. Bettonvil, J. Correira, M. Gyssens,
C. Hergenrother, T. Heywood, J.-L. Rault,
J. Rendtel, C. Verbeeck, S. de Vet, D. Vida.

IMO Sales

Available from the Treasurer or the Electronic Shop on the IMO Website	€	$
IMO membership, including subscription to WGN Vol. 47 (2019)		
Surface mail	26	32
Air Mail (outside Europe only)	49	60
Electronic subscription only	21	25
Proceedings of the International Meteor Conference on paper		
1990, 1991, 1993, 1995, 1996, 1999, 2000, 2002, 2003, per year	9	12
2007, 2010, 2011, per year	15	20
2012, 2013, 2014, 2015 per year	25	34
Proceedings of the Meteor Orbit Determination Workshop 2006	15	20
Radio Meteor School Proceedings 2005	15	20
Handbook for Meteor Observers	15	20
Meteor Shower Workbook	12	16
Electronic media		
Meteor Beliefs Project ZIP archive	6	8

Fireball on 2018 October 12 from Slovenia

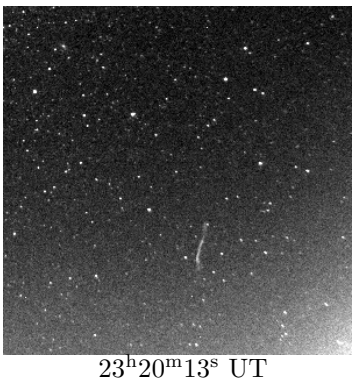

$23^{h}20^{m}13^{s}$ UT

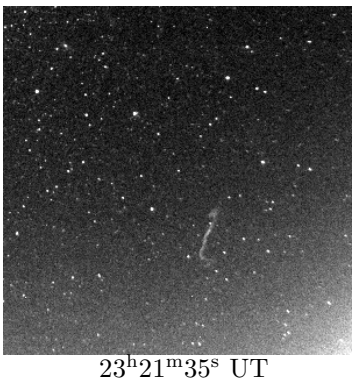

$23^{h}21^{m}35^{s}$ UT

$23^{h}23^{m}07^{s}$ UT

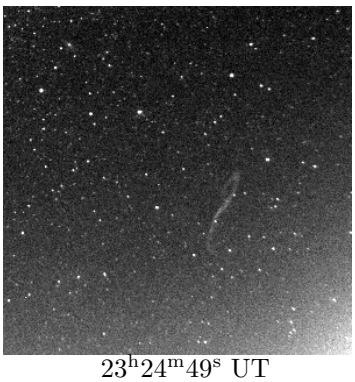

$23^{h}24^{m}49^{s}$ UT

This bright fireball of estimated magnitude -9 occurred on 2018 October 12 at $23^{h}19^{m}20^{s}$ UT. It left a persistent train that was visible for 35 minutes on an all-sky image. Images below show the train evolution during the first 5 minutes. The time mark below each image denotes the mid-exposure time. All images were exposed for 45 seconds. Photo courtesy: Javor Kac/Rezman Observatory.